การศึกษาโครงสร้างและสังเคราะห์โมเลกุลซิฟเบสที่เชื่อมต่อโรดามีนสำหรับการตรวจจับไอออนโลหะหนักด้วยเทคนิคทางฟลูออเรสเซนต์

SCHIFF BASE MOLECULE FUNCTIONALIZED WITH RHODAMINE AS FLUORESCENT DETECTION FOR HEAVY METAL IONS: SYNTHESIS AND MOLECULAR STRUCTURE THEORY

คุณานนต์ ฉัตรไตรรัตน์
KUNANON CHATTRAIRAT

วิทยานิพนธ์นี้เป็นส่วนหนึ่งของการศึกษาตามหลักสูตรวิทยาศาสตรมหาบัณฑิต
สาขาวิชานาโนวิทยาและนาโนเทคโนโลยี
วิทยาลัยนาโนเทคโนโลยีพระจอมเกล้าลาดกระบัง
สถาบันเทคโนโลยีพระจอมเกล้าเจ้าคุณทหารลาดกระบัง
พ.ศ. 2561
KMITL-2018-NT-M-001-006

การศึกษาโครงสร้างและสังเคราะห์โมเลกุลซิฟเบสที่เชื่อมต่อโรดามีนสำหรับการตรวจจับไอออนโลหะหนักด้วยเทคนิคทางฟลูออเรสเซนต์

SCHIFF BASE MOLECULE FUNCTIONALIZED WITH RHODAMINE AS FLUORESCENT DETECTION FOR HEAVY METAL IONS: SYNTHESIS AND MOLECULAR STRUCTURE THEORY

คุณานนต์ ฉัตรไตรรัตน์

KUNANON CHATTRAIRAT

วิทยานิพนธ์เป็นส่วนหนึ่งของการศึกษาตามหลักสูตรวิทยาศาสตรมหาบัณฑิต

สาขาวิชานาโนวิทยาและนาโนเทคโนโลยี

วิทยาลัยนาโนเทคโนโลยีพระจอมเกล้าลาดกระบัง

สถาบันเทคโนโลยีพระจอมเกล้าเจ้าคุณทหารลาดกระบัง

พ.ศ. 2560

KMITL

KMITL-2018-NT-M-001-006

SCHIFF BASE MOLECULE FUNCTIONALIZED WITH RHODAMINE AS FLUORESCENT DETECTION FOR HEAVY METAL IONS: SYNTHESIS AND MOLECULAR STRUCTURE THEORY

KUNANON CHATTRAIRAT

A THESIS SUBMTTED IN PARTIAL FULFILLMENT

OF THE REQUIREMENT FOR THE DEGREE OF

MASTER OF SCIENCE

IN NANOSCIENCE AND NANOTECHNOLOGY

COLLEGE OF NANOTECHNOLOGY

KING MONGKUT'S INSTITUTE OF TECHNOLOGY LADKRABANG

2017

KMITL-2018-NT-M-001-006

Thesis Title	Schiff Base Molecule Functionalized with Rhodamine as Fluorescent Detection for Heavy Metal Ions: Synthesis and Molecular Structure Theory
Student	Kunanon Chattrairat
Student ID	60607007
Degree	Master of Science
Program	Nanoscience and Nanotechnology
Year	2017
Advisor	Asst.Prof.Dr.Darinee Phromyothin

ABSTRACT

Heavy metal ions have been concerned for long time by many organizations i.e., “World Health Organization (WHO). Their toxicities can affect to both of short-term and long-term diseases such as Alzheimer’s disease and Parkinson's disease. Thus, easy and fast measurement has been highly gained attention. Owing to naked-eyes observation and fast response, a fluorescence technique is suitable for heavy metal ion detection. However, designing effective ligand is still challenging to be good selectivity and sensitivity. Thus, molecular structure study is significant to design and investigate structure properties by theoretical calculation. Density functional theory (DFT), is one of the most popular and successful quantum mechanical approaches, has been widely used to calculate and determine the properties such as electronic, optical and physical properties. Therefore, this study uses DFT and time dependent density functional theory (TD-DFT) for investigation of fluorescent ligand properties which is based on Schiff base (SB) molecule owing to easy synthesis and good to interact with metal ion. The calculation was performed by investigating molecular structure in ratio 1:1 and 2:1 of SB and metal ion and its binding site. Moreover, the SB molecule was functionalized with Rhodamine 6G, high molar absorption coefficient and fluorescence quantum yield, to improve optical property. The study was carried

out not only in theoretical study, but also in experiment. In experimental study, synthesis of SB functionalized with Rhodamine 6G (SB-Rho) was carried out. The molecular structure was confirmed by FTIR, ^{1}H NMR. Methanol: DI: ethylacetate in ratio 1:1:1 solvation exhibits the highest fluorescence and completely dissolves SB-Rho. Additionally, anion effect was performed by using iron complexes. The anion has no effect to SB-Rho fluorescence. The heavy metal ion detection with SB-Rho was carried out using various heavy metal ion. The results indicate that only manganese (II) ion is quenching fluorescent intensity with linear calibration curve at 100-500 μM and LOD is 7 μM. The job's plot illustrates the ratio 2:1 of SB-Rho and manganese (II) ion.

Keywords: Density functional theory, Schiff base molecule, heavy metal ion, fluorescent detection

หัวข้อวิทยานิพนธ์	การศึกษาโครงสร้างและสังเคราะห์โมเลกุลซิฟเบสที่เชื่อมต่อโรดามีนสำหรับการตรวจจับไอออนโลหะหนักด้วยเทคนิคทางฟลูออเรสเซนต์
นักศึกษา	นายคุณานนต์ ฉัตรไตรรัตน์
ประจำตัว	60607007
ปริญญา	วิทยาศาสตรมหาบัณฑิต
สาขาวิชา	นาโนวิทยาและนาโนเทคโนโลยี
พ.ศ.	2560
อาจารย์ที่ปรึกษา	ผศ.ดร. ดารินี พรหมโยธิน

บทคัดย่อ

ในปัจจุบันองค์กรด้านสุขภาพระดับโลกได้เข้ามามีบทบาทสำคัญในการจัดการปัญหาด้านการปนเปื้อนและอันตรายจากไอออนของโลหะหนักซึ่งโลหะหนักสามารถก่อให้เกิดโรคต่าง ๆ ได้ทั้งในโรคที่เกิดในระยะสั้นและในระยะยาวอย่างเช่น โรคอัลไซเมอร์ และพาร์กินสัน เป็นต้น ดังนั้นการตรวจวัดไอออนของโลหะหนักที่ง่ายและรวดเร็วจึงได้รับความสนใจเป็นอย่างมาก ซึ่งเทคนิคฟลูออเรสเซนต์เป็นวิธีที่สามารถตรวจวัดไอออนของโลหะหนักและตรวจสอบได้ด้วยตาเปล่าอีกทั้งยังสามารถตอบสนองได้อย่างรวดเร็ว ดังนั้นเทคนิคฟลูออเรสเซนต์จึงนิยมนำมาใช้ในการตรวจสอบไอออนของโลหะหนัก อย่างไรก็ตามในการออกแบบโครงสร้างโมเลกุลฟลูออเรสเซนต์เพื่อตรวจจับไอออนของโลหะหนักเพื่อให้มีความจำเพาะเจาะจงและการตอบสนองที่ดียังมีความท้าทาย ดังนั้นการออกแบบโครงสร้างโมเลกุลฟลูออเรสเซนต์และการศึกษาคุณสมบัติเชิงโครงสร้างโมเลกุลโดยใช้การคำนวณทางทฤษฎีจึงมีความสำคัญ ซึ่งทฤษฎีฟังก์ชันนัลความหนาแน่นคือการคำนวณทางควอนตัมถูกนำมาใช้อย่างกว้างขวาง เพื่อคำนวณและทำนายคุณสมบัติต่าง ๆ เช่น สมบัติทางอิเล็กทรอนิกส์ สมบัติทางแสง และสมบัติทางฟิสิกส์ เป็นต้น ดังนั้นในงานวิจัยนี้จึงใช้การคำนวณเพื่อศึกษาสมบัติของโครงสร้างโมเลกุลฟลูออเรสเซนต์ซึ่งใช้โครงสร้างซิฟเบสในการออกแบบ โดยโครงสร้างซิฟเบสเป็นโครงสร้างที่สามารถสังเคราะห์ได้ง่ายและสามารถเกิดอันตรกิริยากับไอออนของโลหะหนักได้จากการมีหมู่ฟังก์ชันที่มีประจุลบ การคำนวณโครงสร้างของซิฟเบสต่อไอออนของโลหะหนักได้มีการศึกษาในอัตราส่วนของซิฟเบสหนึ่งโมเลกุลต่อหนึ่งไอออนของโลหะหนัก และซิฟเบสสองโมเลกุลต่อหนึ่งไอออนของโลหะหนัก เพื่อศึกษาตำแหน่งการเข้าจับของไอออนของโลหะหนัก ยิ่งไปกว่านั้นการปรับปรุงโครงสร้างโมเลกุลซิฟเบสด้วยการเชื่อมต่อกับโรดามีน 6 จี ซึ่งมีสมบัติทางแสงที่โดดเด่น เพื่อให้โมเลกุลซิฟเบสมีสมบัติทางแสงที่ดียิ่งขึ้น นอกเหนือจากการคำนวณทางทฤษฎี ในทางการทดลองได้ทำการสังเคราะห์

โมเลกุลฟังก์ชันซิฟเบสที่เชื่อมต่อกับโรดามีน 6 จี ได้สำเร็จ ซึ่งฟังก์ชันซิฟเบสที่เชื่อมต่อกับโรดามีน 6 จี สามารถละลายได้หมดด้วยสารละลาย 2 ชนิด คือ ไดเมทิลซัลฟอกไซด์ และ เมทานอล: น้ำปราศจากไอออน: เอทิลอะซิเตท ในอัตราส่วน 1:1:1 แต่สารละลายผสมทำให้มีค่าฟลูออเรสเซนต์ที่สูงที่สุด อีกทั้งการตรวจสอบผลกระทบของไอออนลบแสดงให้เห็นว่าไอออนลบไม่มีผลกระทบต่อการเปลี่ยนแปลงตำแหน่งการเปล่งแสงของฟังก์ชันซิฟเบสที่เชื่อมต่อกับโรดามีน 6 จี หลังจากนั้นการตรวจวัดไอออนของโลหะหนักโดยใช้ไอออนของโลหะหนักต่าง ๆ พบว่าเฉพาะแมงกานีส(II)ไอออนสามารถทำให้เกิดการลดลงของสัญญาณฟลูออเรสเซนต์ด้วยความสัมพันธ์เส้นตรงกับความเข้มข้นตั้งแต่ 100-500 ไมโครโมลาร์ ซึ่งค่าต่ำสุดที่สามารถวัดได้ในเชิงปริมาณคือ 7 ไมโครโมลาร์ สุดท้ายการตรวจสอบอัตราส่วนการจับของฟังก์ชันซิฟเบสที่เชื่อมต่อกับโรดามีน 6 จี และ แมงกานีส(II)ไอออน พบว่ามีการจับแมงกานีสไอออนด้วยอัตราส่วน 2:1 คือ 2 โมเลกุลฟังก์ชันซิฟเบสที่เชื่อมต่อกับโรดามีน 6 จี และ 1 แมงกานีส(II)ไอออน

คำสำคัญ: ทฤษฎีฟังก์ชันนัลความหนาแน่น; โมเลกุลซิฟเบส; ไอออนโลหะหนัก; ฟลูออเรสเซนต์

ACKNOWLEDGEMENT

I sincerely appreciate to my thesis advisor, Dr. Darinee Phromyothin for her invaluable help and tremendous supports throughout the course of this research. I am grateful for her because I would not have achieved this far and this thesis would not have been completed without all the support that I have received from her.

I would like to appreciate the supporting from college of nanotechnology, Functional Organic Synthesis Laboratory and Institute for Molecular Science (IMS). I would also like to thank all of staffs at college of nanotechnology, King Mongkut's Institute of Technology Ladkrabang (KMITL) for research facilities.

Finally, I am especially grateful to my family and friends for their advice, encouragement and support throughout my study.

Kunanon Chattrairat

June 2018

CONTENTS

LIST OF FIGURES

LIST OF TABLES

CHAPTER 1

INTRODUCTION

1.1 Statement and significant of the problems

The heavy metal ion is a huge problem in the world. Many organizations highly pay attention for control the pollution from heavy metal ion, for instance, World Health Organization (WHO), and Food and Drug Administration (FDA). Because it takes long time to decompose and can easily dissolved to environmental water. Moreover, it is high toxic for human even low concentration and causes the long-term diseases and disability such as Alzheimer's disease, neurological diseases, and immune system disorders. The lead ions (Pb^{2+}) is extremely hazardous to human leading to impaired intellectual performance. The mercury ions (Hg^{2+}) is also awfully dangerous, it can affect the immune system, alters genetic and enzyme systems, and damage the nervous system. Moreover, nowadays, the small size of nanoparticles (NPs), defined as particles with dimension between 1 and 100 nm, was broadly studied and widely used in many products. As well known, the silver nanoparticles (AgNPs) has widely used in many commercial products, for example, cosmetic, textiles, and house hold items as well as into illegal medical products owing to its antimicrobial properties. Due to the high surface area of metal-based nanoparticles (NPs), it increases the potential to become the metal ions. Due to various hazardous of metal ions, the determination of heavy metal ions is the one of the most importance.

Owing to low cost and less time-consuming method, the theoretical study was highly gained attention for studying many properties such as electronic, optical, and physical properties as well as mechanism of chemical reaction by Density Functional Theory (DFT). Thus, in this work, the Schiff base molecule that containing an imine group which is easiness of preparation, synthetic flexibility, excellent chelating ability has studied by DFT to explain the mechanism of metal ion detection. Additionally, the Time Dependent Density Functional Theory (TD-DFT) has been used to investigate the electronic and optical properties of Schiff base molecule and complexes. However,

this work investigates not only theoretical study but also the experiment. The Schiff base (SB) was synthesized and functionalized with rhodamine 6G to detect the metal ions. By the way, the optical properties of Schiff base when detecting metal ion is not good such as no color changes and low intensity of fluorescence. So, the fluorescent moiety is necessary to enhance optical properties to become a naked-eye detection. Thus, the Schiff base molecule was functionalized with rhodamine 6G (SB-Rho) to enhance the optophysical properties because rhodamine 6G showed a high emission intensity for fluorescence.

1.2 Objectives

There are 2 main objectives of this work that are

1.2.1. To investigate the structure geometries and electronic properties of SB and complexes in ratio of 1:1 and 2:1 with SB to metal ion.

1.2.2. To investigate the structure geometries and optical properties of SB-Rho and complexes

1.2.3. To improve the fluorescent property of Schiff base molecule with rhodamine 6G and undergo the experimental study.

1.3 Process of the study

1.3.1. Comprehension of the structure geometries and electronic properties of Schiff base molecule and complexes.

1.3.2. Investigate the complexes and analyze the properties of SB, SB-Rho and complexes.

1.3.3. Improve the fluorescent property of Schiff base with rhodamine 6G.

1.4 Hypothesis

1.4.1. If the Schiff base molecule can interact to the heavy metal ion, the fluorescent property will be improved by rhodamine 6G for fluorescent detection.

1.4.2. The Complexes between Schiff base and heavy metal ion present good binding energy (BE) and electron delocalization when absorbed photon.

1.4.3. The SB-Rho fluorescent property changes when detect the heavy metal ion.

1.5 Research boundary

In this work, we pay attention to opportunity of Schiff base molecule interacts with metal ions and synthesis of Schiff base molecule functionalized with rhodamine 6G for heavy metal ion detection. The heavy metal ion detection was detected by fluorescent and colorimetric measurement. Thus, SB, SB-Rho and complexes were investigated the structure geometries and electronic properties by DFT and TD-DFT calculation. Moreover, the metal detection was confirmed by the fluorescent and colorimetric methods.

1.6 Expected outcome

1.6.1 Comprehension of synthesis and calculation of Schiff base molecule and complexes.

1.6.2 Functionalized Schiff base molecule with rhodamine 6G to improve the fluorescent detection performance.

1.7 Nomenclature

BE	=	Binding Energy
DI	=	Deionized water
DFT	=	Density Functional Theory
HOMO	=	The Highest Occupied Molecular Orbital
LUMO	=	The Lowest Unoccupied Molecular Orbital
SB	=	Schiff base
SB-Rho	=	Schiff base functionalized with Rhodamine 6G
TD-DFT	=	Time-Dependent Density Functional Theory

CHAPTER 2

LITERATURE REVIEW

2.1 Heavy metal ions

The common toxics from heavy metal, organophosphates and bacterial are a huge problem in human health. The unique presentations of each toxic agents depend on exposure type and exposure time. The heavy metals which by definition are metals having atomic weights between 63.5 and 200.6 $gmol^{-1}$ and a specific gravity greater than 5 gcm^{-3} are the one of the most toxic agents [1]. Even small doses of some essential heavy metals, including copper, iron, lead, manganese, mercury, strontium and zinc are influence both the environment and human health [1, 2]. The heavy metal can be emitted into the environment by natural, mining and industrial. Because these heavy metals are non-biodegradable, ubiquitously distributed [3]. That means heavy metal can cause risk of contamination in soil, water and food chain. However, some of heavy metals were used in food preservation, cosmetic products and manufacturing processes like making of sodium hydroxide [4]. Thus, international organizations such as World Health Organization (WHO) and National Agency for Food and Drugs Administration and Control (NAFDAC) announce heavy metal ions as hazardous substances as shown in Table 2.1 [4, 5]. By the way, the heavy metals can be dissolved by the solution in environment to form the heavy metal ions or organometal. From this reason, the danger not only come from the contamination of heavy metals but also the heavy metal ions. Which can be the neurotoxic and lead to the long-term diseases. Moreover, it also has limitation of heavy metal ions that was announced by international organizations, for example, World Health Organization (WHO) and Bureau of Indian Standards (BIS) are given in Table 2.2. The heavy metal ions also have high toxicity such as lead ion can penetrate through protective blood brain barrier and increase risk of Alzheimer's disease and Senile diseases, Mercury ion can damage the nervous system and inhibit the enzymes and silver ion accumulate and damage tissues and can be genotoxic [6-8]. Manganese ion also found in a wide

variety of dietary sources, including meat, fish, poultry, dried fruit, tea and nuts. The requirement of manganese in humans are very low [9]. Nevertheless, there are reported about parkinsonian effects in who experience low manganese exposures [10, 11]. Furthermore, the Mn(II) is associated with toxicity to mitochondria and is commonly linked to water pollution due to its stability in aqueous systems [12].

Table 2.1 Guideline heavy metals in drinking water by the World Health Organization (WHO) and National Agency for Food and Drugs Administration and Control (NAFDAC), Nigeria.

Heavy metal ions	Max. acceptable conc. (WHO)	Max. acceptable conc. (NAFDAC)
Zinc (Zn)	5 mg/l	5 mg/l
Arsenic (As)	0.01 mg/l	0.0 mg/l
Magnesium (Mg)	50 mg/l	30 mg/l
Calcium (Ca)	50 mg/l	50 mg/l
Cadmium (Cd)	0.003 mg/l	0.0 mg/l
Lead (Pb)	0.01 mg/l	0.0 mg/l
Silver (Ag)	0.0 mg/l	0.0 mg/l
Mercury (Hg)	0.001 mg/l	0.0 mg/l

Table 2.2 Limits of heavy metal ions by World Health Organization (WHO) and Bureau of Indian Standards (BIS).

Heavy metal ions	Max. acceptable conc. (WHO)	Max. acceptable conc. (NAFDAC)
Lead (Pb)	0.05 mg/l	0.05 mg/l
Cadmium (Cd)	0.005 mg/l	0.01 mg/l
Mercury (Hg)	0.001 mg/l	0.001 mg/l
Arsenic (Ar)	0.05 mg/l	0.05 mg/l
Chromium (Cr)	0.05 mg/l	0.05 mg/l
Silver (Ag)	0.1 mg/l	0.1 mg/l
Zinc (Zn)	5 mg/l	5 mg/l

Copper (Cu)	1.3 mg/l	1.3 mg/l

in household products and exposure to human and ecosystem. Actually, silver impacts to the lowest trophic levels first for example bacteria, which are both aerobic and anaerobic bacteria [7]. However, it can transfer and impact to higher organisms as well.

These are many methods to detect the metal ion such as fluorescence, electrochemical method, and chromatography [13-18]. For this study, the fluorescent and colorimetric method was considered for metal ions detection by using Schiff base molecule modified with rhodamine 6G owing to their favorable metal coordination, high fluorescence quantum yield, simply preparation, and easy observation. Additionally, the DFT was used to calculate the Schiff base molecule, functionalized Schiff base molecule, and complexes for determination of optimized molecular structure, optical properties, and fluorescence mechanism.

2.2 Schiff base molecule

Schiff base was first reported by Hugo Schiff in 1864 [19]. Schiff base is carbon-nitrogen double bond with the nitrogen atom connected to an alkyl or aryl group, but not hydrogen. It can be called imine or azomethine. Schiff base are formed between a primary amine reacts with an aldehyde or ketone which the carbonyl group (C=O) has been replaced by an imine or azomethine group as shown in Figure 2.1. The

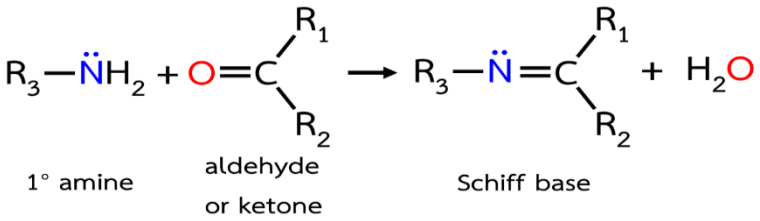

Figure 2.1 General scheme for formation of Schiff base

general formula structure is $R_1R_2C=N-R_3$ where, normally, R_1 is hydrogen atom, R_2 and R_3 are various substituted. Due to various atom and molecular substituted, Schiff base ligands are easily synthesized, formed to desired structure and complexed with almost all metal ions [19, 20]. The Schiff base has many applications in various field for

example biology as anti-bacterial and antifungal activity, pharmacology as anti-cancer, anti-HIV and antioxidant activity [19, 20]. The Schiff base molecule was synthesized by

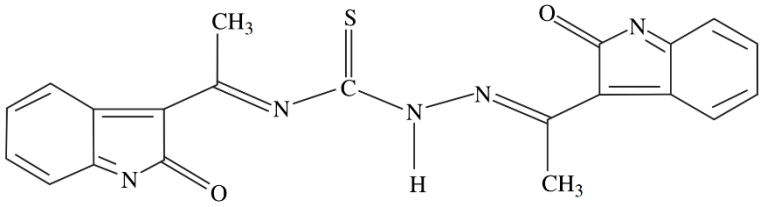

Figure 2.2 The Schiff base structure for antimicrobial activity

condensation of 3-acetyl-oneindol with hydrazinecarbothioamide (2:1) and evaluated for antimicrobial activity by cup-plate method using norfloxacin and griseofulvin as standard [21]. Its structure is shown in Figure 2.2. Moreover, the Schiff base was also used as metal ions detection.

Sapana et al. synthesized cellulose-based materials, including their Schiff bases, as a sensor-adsorbent for highly selective, rapid and simple detection and removal of mercury ions (Hg^{2+}) from aqueous solution. The Hg^{2+} sensing can be observed by

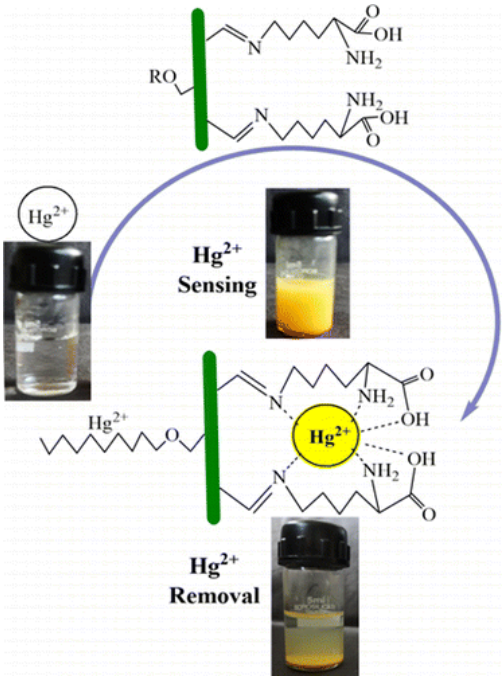

Figure 2.3 The color of Hg(II) solution will change from colorless to yellow when add the sensor-absorbent to solution [22].

naked-eyes and fluorescence spectroscopy. By naked eyes observation, the

transparent Hg^{2+} solution will change the color to yellow when adding the sensor-adsorbent. The intensity of fluorescence increases following the Hg^{2+}concentration from 10-100 ppm. This sensor-adsorbent has very high maximum adsorption capacity of 258.75 mgg^{-1}. In their work, the kinetic and isotherm models were analyzed for Hg^{2+} adsorption as well. The color of solution changes when it detects the Hg^{2+} as presented in Figure 2.3 [22].

Other one for heavy metal ions detection, Sudhir *et al*. designed and synthesized two new Schiff base receptors as shown in Figure 2.4 for selective aluminium ions (Al^{3+}) detection. Both the receptors show colorimetric activity and large

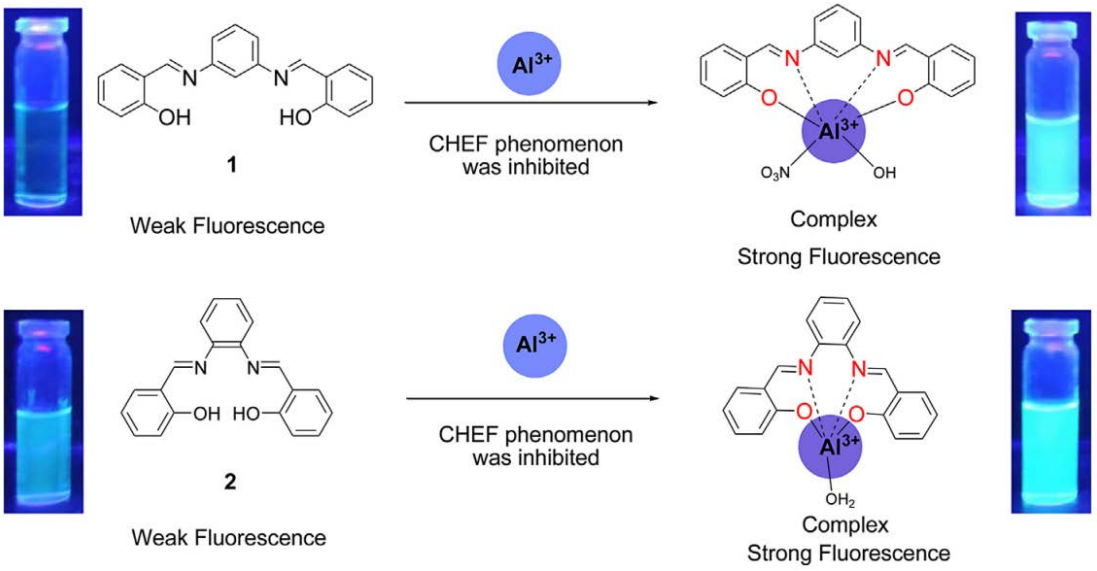

Figure 2.4 The possible mechanism of Al^{3+} detection [23]

fluorescence enhancement as "ON-OFF" fluorescent type after addition of Al^{3+}. Figure 2.4 show the possible mechanism of both receptors fluorescent behavior which demonstrate the Al^{3+} detection. The detection limit was found to be 4.79 x 10^{-8} M and 8.28 x 10^{-8} M for receptors 1 and 2, respectively [23].

The Schiff base group was also studied by Density Functional Theory (DFT). Pritam *et al.* reported that anion sensor was performed by synthesis of two new Schiff base molecules which -NO_2 substituted (P1) and -CN substituted (P2) for sensing F^-, OAc^- and $H_2PO_4^-$ and only F^-, respectively. They demonstrate the fluorescence "ON-OFF" responses for F^- detection. Moreover, the test kit was fabricated by operate the

logic on electronic circuit based on XNOR, XOR, OR, AND, NOT and NOR logic operations to design option "Write-Read-Erase-Read". By the way, the ^{1}H-NMR results of P1 and P2 which form HF_2^- were observed that were different. So, to achieve insight in host-guest interaction and to find out the detail of the complexation of sensor and sensing anions, the DFT calculation has been taken into consideration [15].

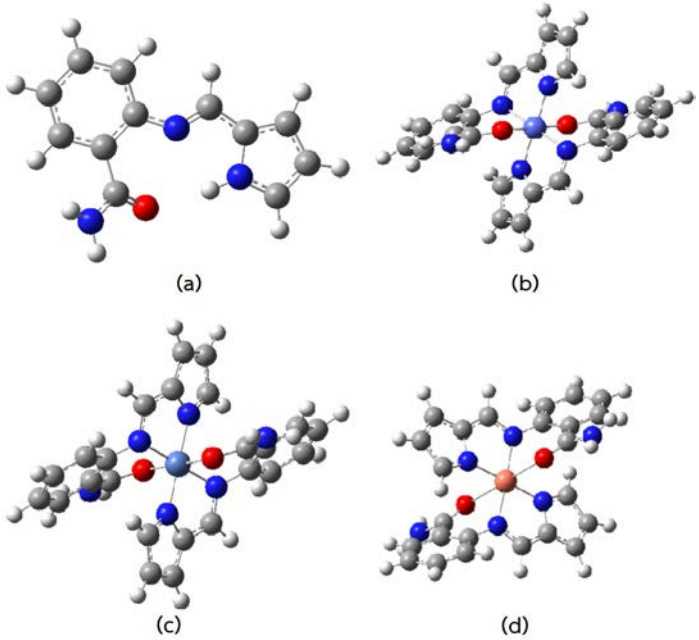

Figure 2.5 Geometry optimized structures of (a) ligand **L^1**, (b) Co^{2+}complex, (c) Ni^{2+} complex, and (d) Cu^{2+} complex [24]

A series of two active Schiff base ligands **L^1**, **L^2** have been synthesized in reaction of 2-aminobenzamide with pyrrol-2-carboxaldehyde and furan-2-carboxaldehyde by Prateek [24]. Which was used for complexation with metal ions (Co^{2+}, Ni^{2+} and Cu^{2+}) by ratio of ligand: metal as 2:1. ^{1}H NMR, UV-Vis, TGA, IR, mass spectrophotometry, EPR and molar conductivity were used to characterize the complexes. Then all the synthesized compounds were studied for *in vitro* antimicrobial activities by using serial dilution method. Moreover, the theoretical study was used to investigate the geometries of Schiff base and metal complexes by DFT with fully optimized using the 6-31+g(d,p) basis set as shown in Figure 2.5. The results elucidate octahedral geometry for Co^{2+} and Ni^{2+} complexes and distorted octahedral geometry for Cu^{2+} complexes.

2.3 Rhodamine

Rhodamine was hugely gained and widely used as fluorescent probes owing to their high absorption coefficient, fluorescence in the visible region of electromagnetic spectrum, high fluorescence quantum yield and photostability [25, 26]. The structure of rhodamine belongs to the family of xanthenes as shown in Figure

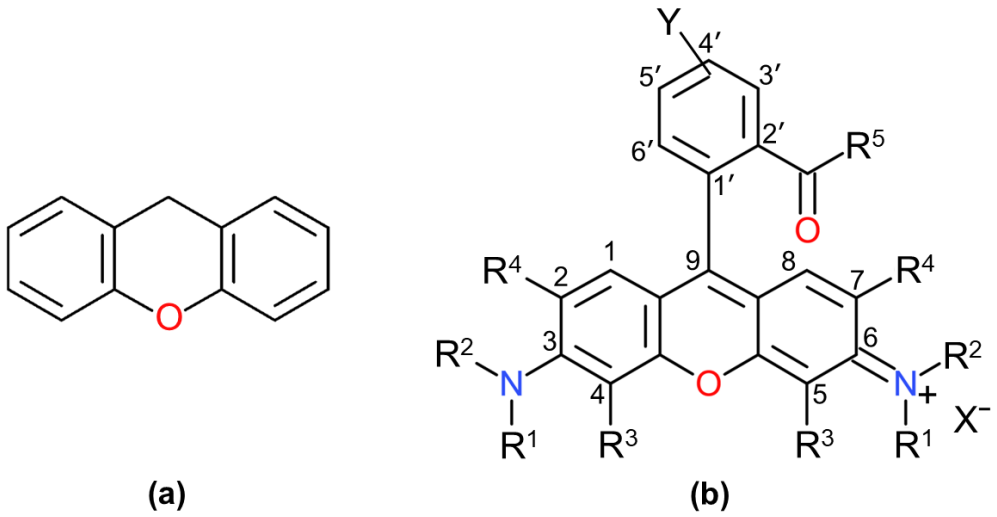

Figure 2.6 Molecular structure of (a) xanthene and (b) rhodamine

2.6. It was used in various application such as pro-fluorophores enzymatic activity, labelling of molecules and chemosensor for either *in vitro* and *in vivo* in detection of metal ions, acids and (bio)molecules [25]. Due to various application of rhodamine, the most application, rhodamine needs to be covalently linked to another (bio)molecules or surface. Thus, the modification of rhodamine is necessary depending on the substituents R1, R2, R3, R4, Y and even on the counter ion X^- (usually Cl^-, Br^- or ClO_4^-) as presented in Figure 2.6. The photophysical properties for instance absorption, emission, fluorescence life time (τ) and fluorescence quantum yield (ϕ) are different depending on the solvent and pH [27, 28]. The types of modification of rhodamine derivatives can be divided to three types: modification of the amino groups of xanthene moiety (positions 3 and 6); modification of the carboxyphenyl ring (positions 4' and/or 5') or modification of the carboxylic acid group (position 2'). Owing to various modification of rhodamine, some of commercial molecular rhodamine structures such

as Rhodamine 123 and Rhodamine 116 are expensive as one can see in Table 2.3 [25]. However, Rhodamine B and Rhodamine 6G are the less expensive dyes of the rhodamine derivatives. So, they have been more played important roles for further applications.

Table 2.3 Commercially available rhodamine derivatives [25].

	Structure	€/g[a]
Rhodamine B	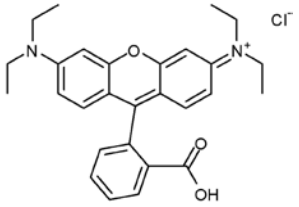	0.45
Rhodamine 6G	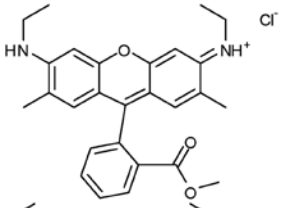	1.60
Rhodamine 19	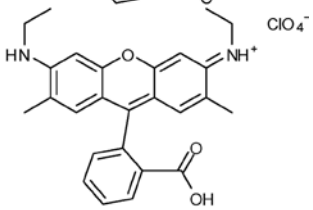	156
Rhodamine 101	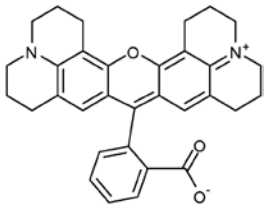	80
Rhodamine 110	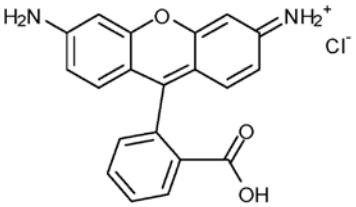	128
Rhodamine 116	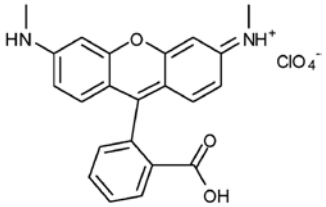	205
Rhodamine 123		1650

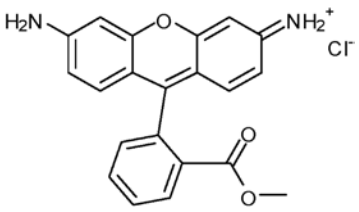

[a] An average for common suppliers: Acros Organics, Aldrich, Alfa Aesar, Fluka, Radiant dyes laser, Sigma.

This work, Rhodamine 6G will be modified at position 2' that seem the easiest to functionalize because it already has a functional group. Nevertheless, the scientific literature after 2000 just began to report the methods of its modification [25]. After the few reports can be found, it was used to develop in various application such as light-screening dyes, biological diagnostic and most of chemosensor application.

Shiguo Sun *et al*. synthesized the rhodamine derivative which is naphthylamine-rhodamine hybrid (RN) for ratiometric and colorimetric fluorescent probe to detect Pd^{2+} ions. The scheme of RN synthesis as illustrated in Figure 2.7,

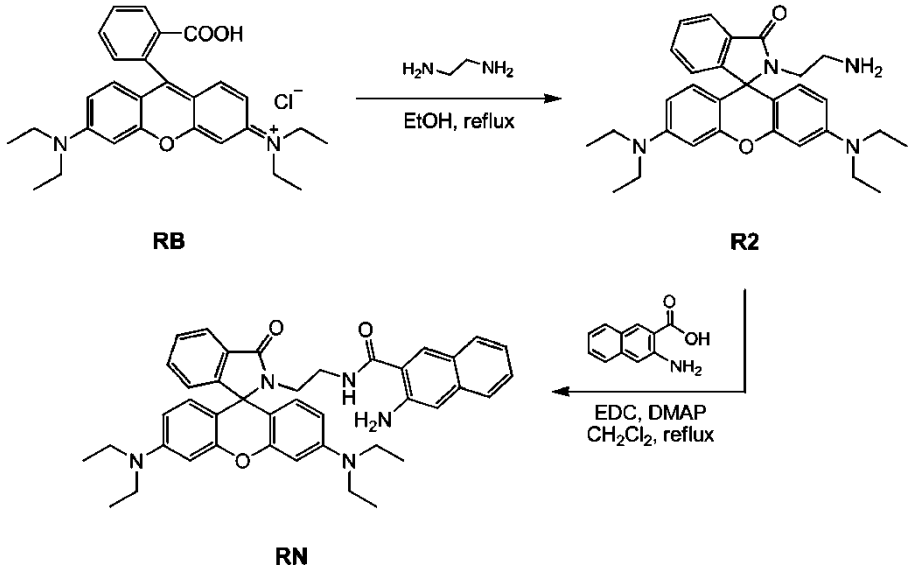

Figure 2.7 The structure and synthesis of RN [28]

firstly, was undergone by using rhodamine B and ethylenediamine as reactants to obtain the intermediate R2. Then, the reaction of R2 with 3-amino-2-naphthoic acid was performed to achieve the probe RN. The fluorescence color of RN is aquamarine blue from naphthylamine moiety. When complex with Pd^{2+}, the aquamarine blue

fluorescence was quenched and the spirolactam ring of rhodamine was opened that lead to appearance of red fluorescence. The RN has high sensitivity and selectivity for Pd^{2+} as shown in Figure 2.8. Moreover, the Pd^{2+} ion in live mice was monitored by the probe with fluorescence imaging [28].

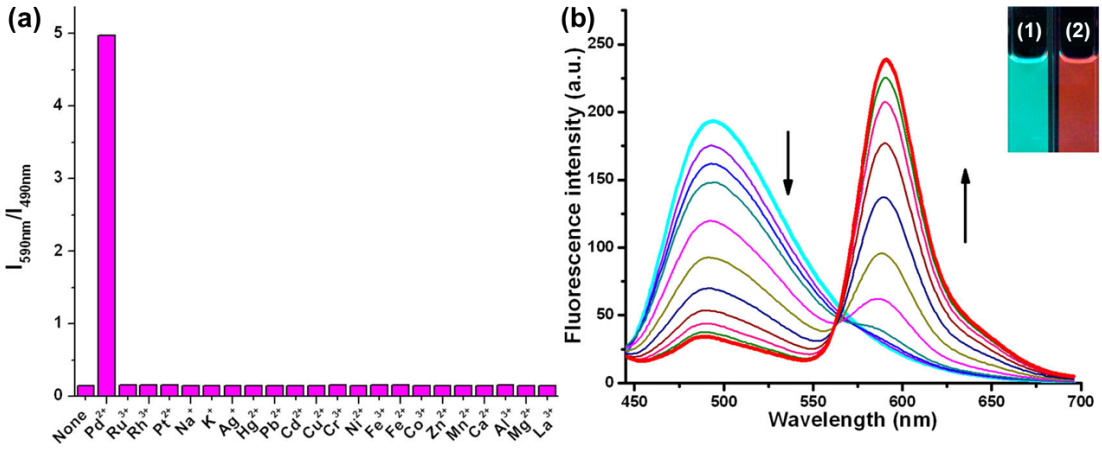

Figure 2.8 (a) Fluorescence intensity ratio ($I_{590\ nm}/I_{490\ nm}$) of RN in the presence of different metal ions (b) Fluorescence spectra of RN upon titration with $PdCl_2$ in EtOH/H_2O (1:1, v/v) at room temperature (1) before and (2) after the addition of $PdCl_2$ [28]

The photoluminescence techniques are the most efficient methods for various analytes detection due to their high sensitivity and selectivity, and high temporal and spatial resolution [29]. Thus, there are extremely attractive in biological and environmental significance which is rapidly applied and developed for detection and imaging of specific molecules, microenvironments, biological processes and events. In the past decade, many photoluminescent probes with various characteristics were reported. The metal coordination of organic dyes plays an essential role in the metal ions sensor owing to its distinct optical responses. The transition metal complexes illustrate unique luminescence properties for different organic dyes such as large stokes shift, long emission wavelength, emission lifetime, high quantum yield.

Lok Nath Neupane *et al*. synthesize fluorescent peptidyl chemosensor for the detection of heavy metal ions in aqueous solution as well as in cells on the basis of the peptide sensor receptor using as aggregation-induced emission fluorophore as known as excimer formation. The peptidyl chemosensor showed a distinctly selective

turn-on response to Hg^{2+} among 16 metal ions in buffer solution containing NaCl. The peptidyl chemosensor complexed with Hg^{2+} and then excimer formation was occurred, resulting in the significant emission (OFF-ON) at around 470 nm. The detection limit (5.3 nM, 1.06 ppb, R^2 = 0.99) of peptidyl chemosensor for Hg^{2+} was lower than the maximum allowable level of Hg^{2+} in drinking water by United States Environmental Protection Agency (10 nM, 2 ppb). Moreover, the peptidyl chemosensor was undergone for intracellular Hg^{2+} detection in RKO cells in aqueous solutions containing 1% DMSO [30].

In addition to photoluminescence technique for metal ions detection, the colorimetric detection is also widely used for distinct change of solution color when detecting the metal ions. Doan Thanh Nhan *et al*. synthesize a benzothiazolium-derived colorimetric and fluorescent chemosensor (L) for mercury ions detection. The detection limits of colorimetric and fluorescent method are lower than the reported chemosensors based on similar derivatives of benzothiazolium of 15.3 and 11.8 ppb, respectively. It has selective detection for mercury ions in presence of competing metal ions, including Cd^{2+}, Fe^{2+}, Co^{3+}, Cu^{2+}, Zn^{2+}, Pb^{2+}, Ca^{2+}, Na^{+} and K^{+} ions. Moreover, B3LYP/LanL2DZ was used for simulation of optimized molecular structures, absorption and fluorescence characteristics of chemosensor and its complex. Resulting in the formation of Hg_2L_2 complex occurred let to a significant transfer of electron density from ligands to the metal ions and broke the **π**-electron conjugated system. That leads to significant fluorescence quenching and color change in the complex [31].

2.4 Theoretical study

In quantum mechanics, the system can be possibly contained in the system's wave function, Ψ. The nuclear degrees of freedom appear only in the form of a potential **V**(**r**) acting on the electron [32]. So, this wave function is calculated from Schrödinger's equation, which for a single electron, nonrelativistically, moving in a potential **V**(**r**) reads

$$\left[-\frac{\hbar^2\nabla^2}{2m}+v(r)\right]\psi(r)=\ \varepsilon\psi(r). \tag{2.1}$$

If there is more than one electron Schrödinger's equation becomes

$$\left[\sum_i^N(-\frac{\hbar^2\nabla^2}{2m}+v(r_i)+\sum_{i<j}U(r_i,r_j)\right]\psi(r_1,r_2,\dots,r_N) = E\psi(r_1,r_2,\dots,r_N), \tag{2.2}$$

where N is the number of electrons and U($\mathbf{r}_i$, $\mathbf{r}_j$) is the electron – electron interaction. For a coulomb system has

$$\hat{\mathrm{U}}=\ \sum_{i<j}U(r_i,r_j)=\sum_{i<j}\frac{q^2}{|r_i-r_j|}. \tag{2.3}$$

The kinetic energy operator, as the same operator for any system of particles interacting via the Coulomb interactions, is the same for any nonrelativistic system.

$$\hat{T}=-\frac{\hbar^2}{2m}\sum_i\nabla_i^2 \tag{2.4}$$

The sequence which usual quantum mechanical approach to Schrödinger's equation (SE) can be summarized.

$$v(r)\overset{SE}{\Rightarrow}\psi(r_1,r_2,\dots,r_N)\overset{\langle\psi|\dots|\psi\rangle}{\Longrightarrow}observables \tag{2.5}$$

i.e., one specifies the system by selecting **V**(**r**), puts it into Schrödinger's equation, solves for the wave function Ψ and then calculates observables by taking expectation

values of operators with this wave function. One among the observables that are calculated in this way is the particle density

$$n(r) = N \int d^3r_2 \int d^3r_3 \dots \int d^3r_N \, \psi^*(r_1, r_2, \dots, r_N)\psi(r_1, r_2, \dots, r_N) \quad (2.6)$$

The Schrödinger's equation, powerful methods, have been developed however it struggles with many-body problem. Nobody has ever calculated the chemical properties of a 100-atom molecule with full configuration interaction (CI) which is diagrammatic perturbation theory (based on Feynman diagrams and Green's functions). There is density functional theory (DFT) provides a viable alternative, less accurate probably, but much more versatile. DFT clearly concedes that nonrelativistic Coulomb systems differ only by their potential **V**(**r**). Furthermore, DFT provides a way to systematically map the many-body problem onto a single-body problem. All this is done by promoting the particle density n(r). Most of properties i.e., electrical, magnetic, and structural properties of materials have been calculated using DFT. The density-functional approach can be summarized by the sequence

$$n(r) \Rightarrow \psi(r_1, \dots, r_N) \Rightarrow v(r), \quad (2.7)$$

i.e., cognition of n(r) implies cognition of the wave function and the potential, and thus of all other observables. The heart of DFT is the Hohenberg-Kohn (HK) theorem. This theorem can be inverted: provided a ground-state density $n_0(r)$ it is possible, to calculate the corresponding ground-state wave function $\Psi_0(r_1, r_2, \dots, r_N)$. This means that attend that Ψ_0 is a functional of n_0. Therefore, all ground-state observables are functional of n_0 as well. The cognition of $n_0(r)$ implies exact cognition of an arbitrary function f(r). The ground-state wave function Ψ_0 is not only reproduce the ground-state density, but also minimize the energy. For a provided ground-state density $n_0(r)$, the equation can be written as

$$E_{v,0} = \min_{\psi \to n_0} \langle \psi | \hat{T} + \hat{U} + \hat{V} | \psi \rangle, \quad (2.8)$$

where $E_{v,0}$ is the ground-state energy in potential **V**(**r**). The equation informs that for a provided density $n_0(r)$ the ground-state wave function Ψ_0 is that which reproduces this

$n_0(r)$ and minimizes the energy. For an arbitrary density n(r), functional equation can be defined

$$E_v[n] = \min_{\psi \to n} \langle \psi | \hat{T} + \hat{U} + \hat{V} | \psi \rangle. \quad (2.9)$$

Where n is a density different from the ground-state density n0 in potential **V**(**r**), then the Ψ that produce this n are different from the ground-state wave function Ψ_0, and according to the variational principle the minimum obtained from $E_v[n]$ is higher than or equal to the ground-state energy $E_{v,0} = E_v[n_0]$. Thus, the functional $E_v[n]$ is minimized by the groud-state density n_0, and its value at the minimum is $E_{v,0}$.

The self-consistent field (SCF) calculation was performed following the Figure 2.9. Initially, density was speculated, then, plugs into the Kohn-Sham equation to solve for wave function. After solving wavefunction, the new density is repetitively calculated into Kohn-Sham equation. The procedure is repeatedly calculated until density is convergence or acceptable tolerance.

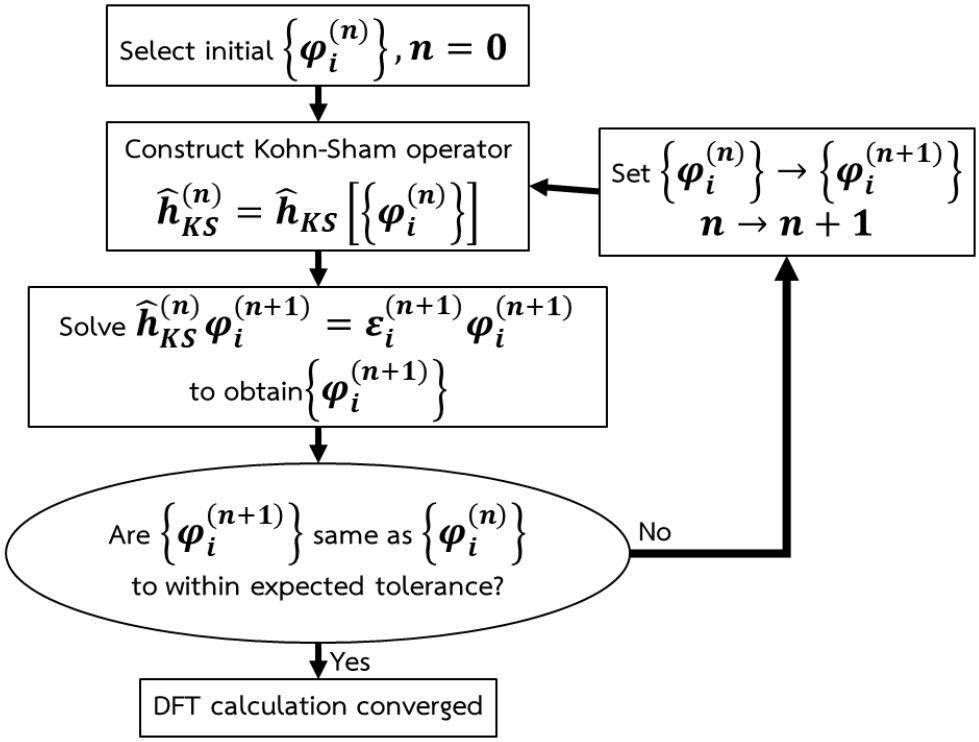

Figure 2.9 The flow chart of self-consistent field (SCF) calculation.

The DFT has been used to calculate the ligand which used as fluorescence sensor. Anna Amat et al. was used DFT and TD-DFT to study the photophysical and photochemical properties of alizarin a fluorescent organic red dye of the family of the anthraquinones, in 2 molecular structures: ALZ and ALZ_PT as illustrated in Figure 2.10. B3LYP as exchange-correlation functional and 6-31g** basis set were used and confirmed both ALZ and ALZ_PT are stable in S_1 (excited state). In ethanol, ALZ is more stable by 0.20 kcal/mol, but, in benzene, ALZ_PT is more stable by 1.40 kcal/mol. ALZ_PT emission energies are almost insensitive to the solvent polarity,

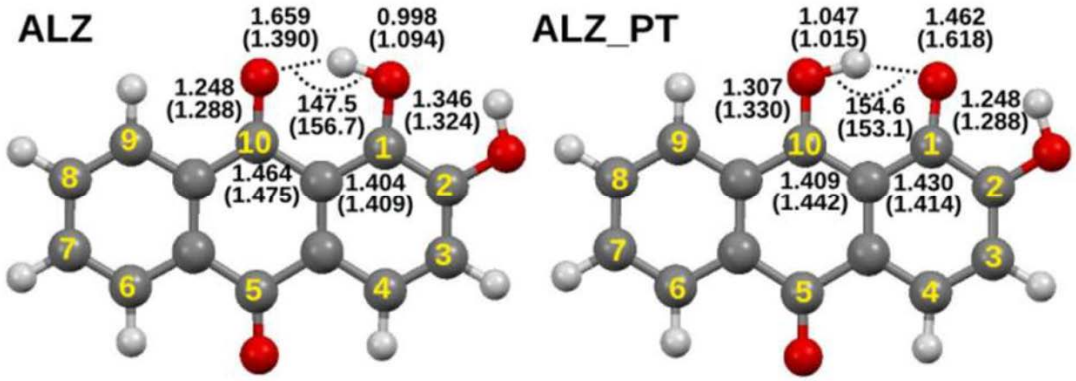

Figure 2.10 Optimized molecular structures of ALZ and ALZ_PT.
(bond length in Å and angles in degrees) [33]

while the ALZ ones are red-shifted when passing from benzene to ethanol. The calculated emission is in good agreement with the retrieved experimental bands which emit in a double band emission spectrum with peaks centered at 610 and 540 nm. ALZ_PT increasing the relative intensity of the experimental emission band between 610 and 690 nm. On the other hand, the experimental band between 525 and 575 nm is compatible with the computed spectra of the ALZ [33].

CHAPTER 3

RESEARCH METHODOLOGY

3.1 Theoretical study

The quantum chemical calculation was brought to investigate the structure geometries and electronic properties of Schiff base molecule (SB) and complexes. All complexes were carried out based on density functional theory (DFT) at all electron level using Gaussian09 [34]. The Schiff base molecule was complexed with heavy metal ion in ratio of 1:1 and 2:1. Then the ground state geometries in vacuum were fully optimized using hybrid functional B3LYP with 6-311G(d,p) basis set for C, H, O, N and S atom and LANL2DZ for heavy metal ions to determine the stable conformation. SB was designed which contain 21 atoms (8 carbon atoms, 2 sulfur atoms, 4 nitrogen atoms, 1 oxygen atom and 6 hydrogen atoms) as shown in Figure 3.1. After the ground state geometries optimization, the electronic properties, binding energy (BE), absorbance spectra, density of states (DOS), the energy of the lowest unoccupied molecular orbital (LUMO), the energy of the highest occupied molecular orbital (HOMO), energy gap were investigated by time-dependence density functional theory (TD-DFT). The BE of the Schiff base complexed with heavy metal ions are calculated using the following eq. 3.1.

$$\text{Binding Energy (BE)} = E^{opt}_{complex} - E^{opt}_{\text{Schiff base molecule}} - E^{opt}_{\text{Heavy metal ion}} \quad \textbf{(3.1)}$$

Here, $E^{opt}_{complex}$ represents the energy of the optimized structure of Schiff base complexed with heavy metal ion. The $E^{opt}_{\text{Schiff base molecule}}$ and $E^{opt}_{\text{Heavy metal ion}}$ represent the energy of the optimized structure of Schiff base molecule and heavy metal ion, respectively. After the ground state calculation had been investigated, the excited state was calculated by using time dependent density functional theory (TD-DFT) with the similar basis set of ground state calculation. Then the fluorescent spectra and electron density were analyzed.

Furthermore, SB was functionalized with Rhodamine 6G (Rho) to improve the optical properties as shown in Figure 3.1. The fully ground state optimization of Schiff base-Rhodamine 6G (SB-Rho) was performed by B3LYP, M06-2X, PBE1PBE, TPSSH, and wB97-XD with 6-311G(d,p) and LANL2DZ basis set to obtain the suitable functional for this complex. Then, the excited state optimization was carried out by TD-DFT with suitable functional to determine the optical properties.

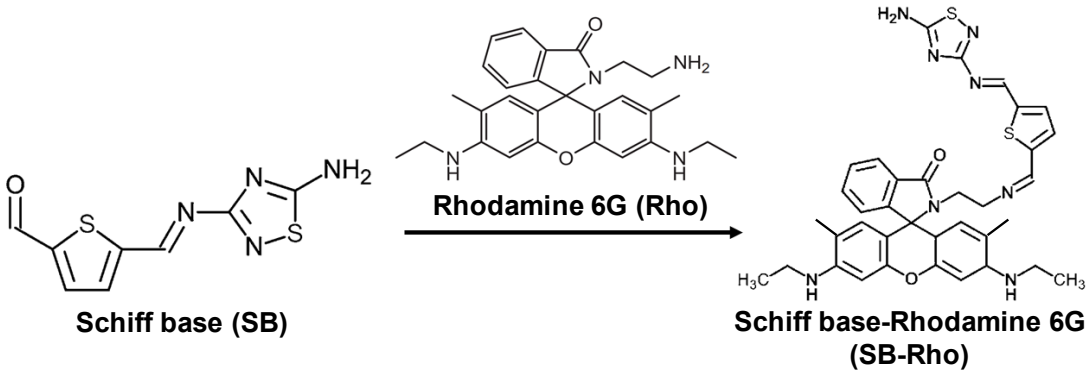

Figure 3.1 The scheme of synthesis SB-Rho

3.2 Experimental study

3.2.1 Materials

Analytical purity of reagents was used in all the experiment. Methanol, ethanol, ethyl acetate and acetonitrile were purchased from Sigma-aldrich. Ethylenediamine was purchased from Fluka. The heavy metals which were used in this study were silver nitrate ($AgNO_3$), cadmium chloride ($CdCl_2$), cobalt(II) nitrate ($Co(NO_3)_2$), Copper(I) iodid, mercuric acetate ($C_4H_6HgO_4$), iron(II) acetate ($C_4H_6FeO_4$), iron(II) chloride ($FeCl_2$), iron(III) oxide (Fe_2O_3), iron(II) sulfate ($FeSO_4$), manganese acetate ($C_4H_6MnO_4$), nickel(II) chloride ($NiCl_2$), lead acetate ($C_4H_6PbO_4$) and zinc sulfate ($ZnSO_4$). All heavy metals were purchased from Sigma-aldrich. The mix solvent was prepared in ratio of 1:1:1 of methanol: DI: ethylacetate.

3.2.2. Apparatus

UV-Vis spectroscope and fluorescent spectroscope were performed using PG instruments T92+ and HORIBA fluoromax plus, respectively. All optical properties were measured at room temperature. All fluorescent measurements were recorded by using slit 2 nm, excitation at 350 nm and integral time 0.2 sec. ^{1}H Nuclear magnetic resonance (NMR) spectra were recorded with an INOVA VARIAN 400 MHz spectrometer. Fourier-transform infrared spectroscope (FTIR) was recorded with Perkin Elmer model spectrum two.

3.2.3 Preparation of rhodamine 6G-ethylenediamine

Figure 3.2 shows the schematic synthesis of SB-Rho. Firstly, The preparation of rhodamine 6G-ethylenediamine, the Rhodamine 6G (958 mg, 2 mmol) was dissolved in 20 mL of ethanol. Then 1 ml of ethylenediamine (15 mmol) was added to the solution. The reaction was refluxed for 4 hours at 60 °C until the color of solution disappears. After that the precipitate was collected and washed with absolute ethanol for three times. The product was purified by recrystallization from acetonitrile to give

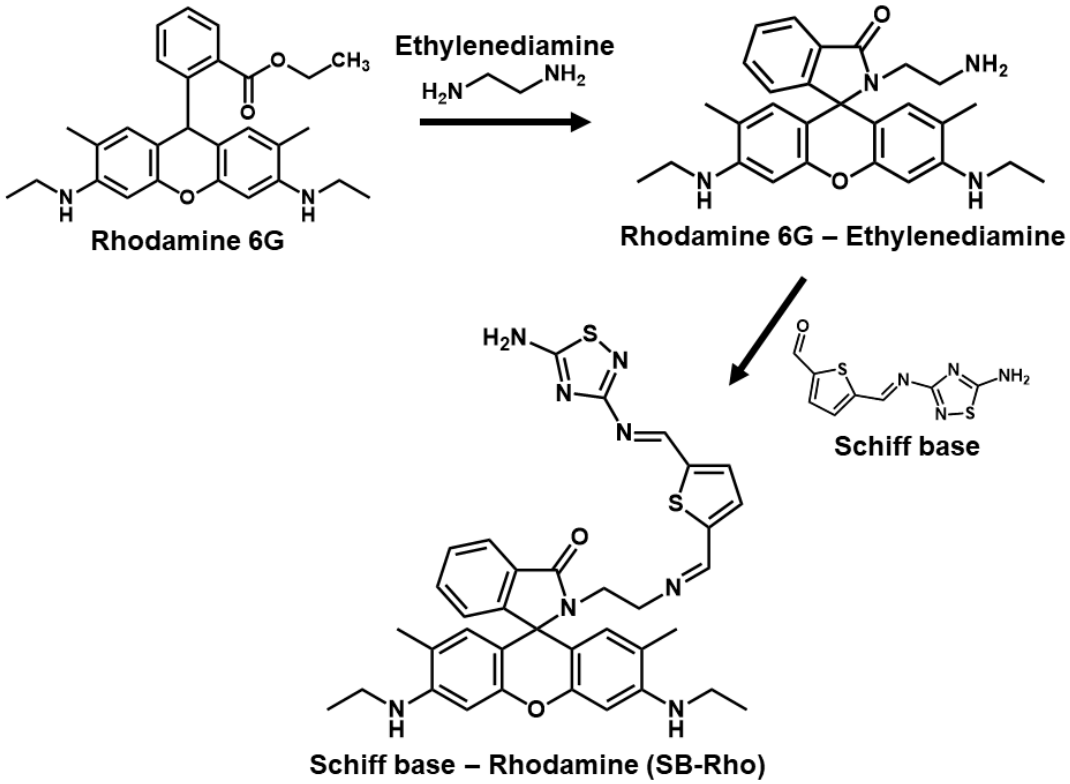

Figure 3.2 The schematic synthesis of Schiff base – rhodamine 6G (SB-Rho)

rhodamine 6G-ethylenediamine (white solid). Then the characterization was performed by FTIR, NMR and UV-Vis spectroscope.

3.2.4 Synthesis of SB-Rhodamine (SB-Rho)

The Schiff base molecule was synthesized as illustrated in Figure 3.3. 2,5-thiophenedicarboxylaldehyde and 1,2,4-thidadiazole-3,5-diamine with the ratio of 1:1 in ethanol were mixed and carried out under reflux for 3-5 h at 50 °C. After the reaction, evaporation process and purification with ethanol was undergone to eliminate the solvent and impurity, respectively. Then, the yellow powder was collected and characterized [35]. After SB was successfully synthesized, SB has been functionalized with rhodamine 6G-ethylenediamine as shown in Figure 3.2. The rhodamine 6G-ethylenediamine and Schiff base were dissolved in 30 mL in ethanol. Then the reaction was refluxed for 6 hours at 60 °C under nitrogen atmosphere and stirred for 2 hours at

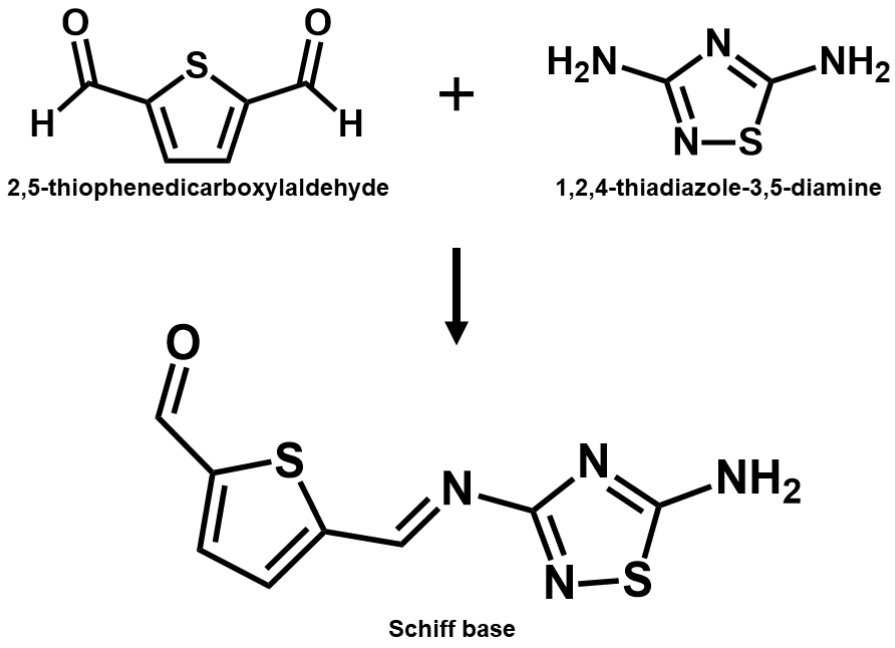

Figure 3.3 The schematic synthesis of Schiff base (SB)

room temperature. Then the precipitate was washed with absolute ethanol 3 times. The recrystallization was performed by absolute ethanol. After that, the metal ion

detection was tested by add the SB-Rho solution to heavy metal ions solution of ratio 1:1. The characterization was performed by fluorescence, UV-Vis, FTIR and NMR.

3.2.5 Heavy metal detection by SB-Rho

The solvent effect was performed by using various solvent (aceton, acetonitrile, dimethylsulfoxide, ethanol, ethylacetate, methanol, methanol: DI, methanol: ethylacetate, ethylacetate: DI, methanol: DI: ethaylacetate). The mixed solvents were used in ratio of 1:1 and 1:1:1 in all solvents. 0.2 mM of SB-Rho in methanol: DI: ethylacetate has the highest fluorescence intensity among solvents. After that, methanol: DI: ethylacetate was used to investigate the metal ion. The anion effect was tested by iron complex with various anion (Cl^-, $COOH^-$, NO_3^-, SO_4^{2-}). Then, 1 mM stock solutions of heavy metal ions and 0.2 mM SB-Rho were prepared in mix solvent (1:1:1 of methanol: DI: ethylacetate). The solutions were diluted to 400 μM with mix solvent. Then, 80 μl SB-Rho was added to total volume 2 ml. Then, the various heavy metal ions were measured with SB-Rho by using equal concentration at 0.1 μM. All absorption and emission spectra were performed in a quartz optical cell of 1 cm optical path length at room temperature. All fluorescence measurement was carried out using excitation at 350 nm. Both excitation and emission slit widths were 1 nm and integral time 0.2 sec.

CHAPTER 4

RESULTS AND DISCUSSION

4.1 Theoretical study

In this work, the theoretical calculation was divided in 3 parts. The first part is investigation of complex between 1:1 of SB to metal ion to find the binding site of metal ion. The second part is an investigation of complex that include 2:1 of SB to metal ion because this orientation probably occurs by natural structure of SB molecule. Finally, the third part is the calculation of complex between SB molecule functionalized with Rhodamine 6G (SB-Rho) and heavy metal ions. Additionally, the electron distribution, absorption and emission spectra were calculated to predict the optical properties of SB-Rho and mechanism.

4.1.1 Investigation of 1:1 of SB molecule to metal ion

The SB molecule was designed following the previous literature [36]. They tried to coat carbon paste electrode (CPE) and Printed circuit board (PCB) gold electrode with this SB molecule for silver ion (Ag^+) detection by electrochemical method. For this work, the binding site of Ag^+ was investigated by DFT with B3LYP functional using 6-311G(d,p) and LANL2DZ basis sets. The positions of binding site were proposed in 3 positions as shown in Figure 4.1(a). Then fully optimizations of complexes were performed to determine the stable orientation. The results show that, after fully optimization, all of input positions was optimized to the first position. That implies the first position is the most stable orientation and the binding site is around the imine group as presented in Figure 4.1(b). Moreover, the binding energies, were calculated following the equation 3.1, clearly illustrate the equal energy as shown in Table 4.1. Additionally, the electrostatic surface potential (ESP) was calculated as shown in Figure 4.2. Red and blue color show the negative and positive electrostatic potential, respectively. The surface area around aldehyde and imine group shows the red color which implies to nucleophilic moiety. So, metal ion can be possibly interacted to SB

at the imine group. Then, the optical properties of complex were investigated in means of absorbance and emission by TD-DFT with B3LYP. However, to optimize the excited state with B3LYP was not success. The wB97X-D, is hybrid functional including the short-range and long-range correction [37], was used to calculate the absorbance and emission of SB and complex. The absorbance (Abs) and emission (Em) of SB and SB with Ag^+ (SB-Ag^+) was calculated as shown in Figure 4.3. The absorption and emission

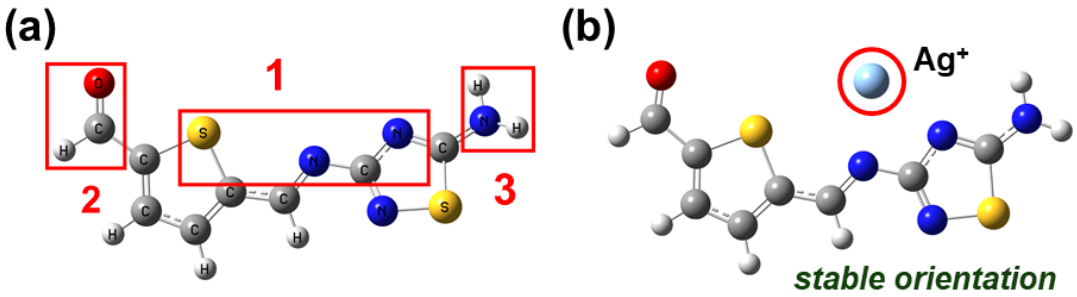

Figure 4.1 (a) The proposed binding position of Ag^+ (b) the binding site at imine group is stable orientation

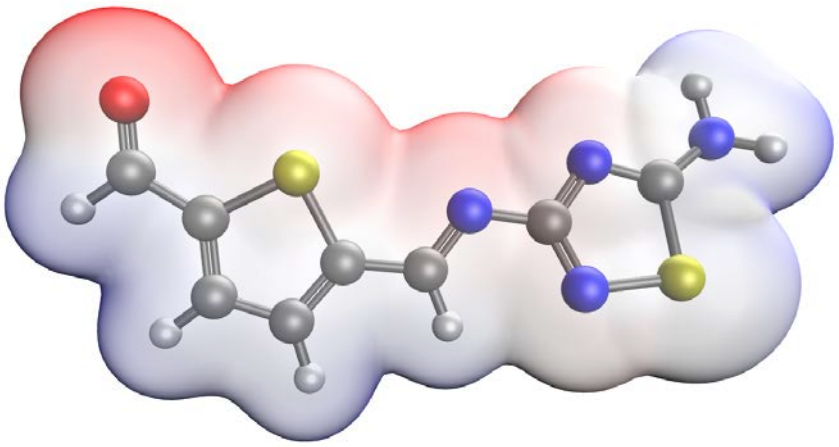

Figure 4.2 The electrostatic surface potential (ESP) of SB

peak of SB is 320 and 332, respectively. When SB interacted with Ag^+, the red-shift was occurred from 320 nm to 335 nm for absorbance and 332 nm to 352 nm for emission. In actually, the 10 nm red-shift was not clearly observed by vision. However, the binding energy and red-shift confirmed the SB can be responded with Ag^+ which was measured with electrochemical technique [36].

Table 4.1 The binding energy and bond length of C=N at imine group.

Position	Binding Energy (BE) (kcal/mol)
1	-63.78
2	-63.78
3	-63.78

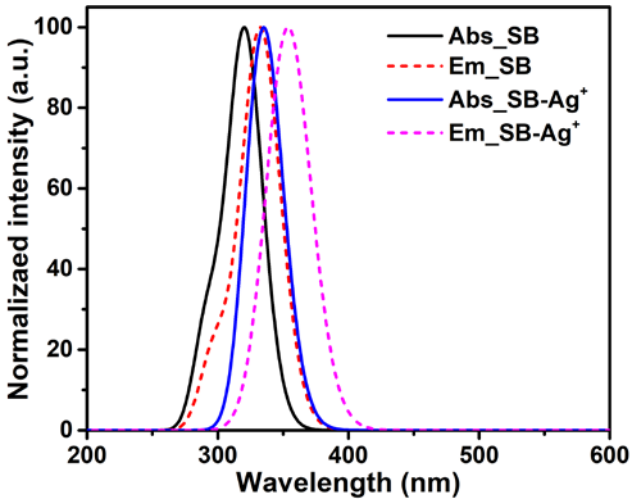

Figure 4.3 The absorbance and emission of SB and SB-Ag^{+}

Table 4.2 Calculated absorption and emission wavelength (**λ**), excitation energies (E) and oscillator strengths (f) of the SB and complexes in gas phase at wB97X-D/6-311G(d,p) and TD-DFT.

	Electronic transitions	E (eV)	**λ** (nm)	*f*	Transition state
Abs_SB	$S_0 \rightarrow S_1$	3.73	332	0.0010	H-3 → L (70%)
	$S_0 \rightarrow S_2$	3.87	320	0.5511	H → L (76%)
	$S_0 \rightarrow S_3$	4.24	292	0.1650	H-4 → L (49%)
Em_SB	$S_0 \rightarrow S_1$	3.16	392	0.0002	H-2 → L (77%)
	$S_0 \rightarrow S_2$	3.72	333	0.6092	H → L (81%)
	$S_0 \rightarrow S_3$	4.16	298	0.1203	H-4 → L (44%)

Abs_SB-Ag^+	$S_0 \rightarrow S_1$	3.45	359	0.0001	H-1→L (68%)
	$S_0 \rightarrow S_2$	3.71	334	0.6194	H→L (84%)
	$S_0 \rightarrow S_3$	4.10	302	0.0005	H → L+1 (93%)
Em_SB-Ag^+	$S_0 \rightarrow S_1$	2.81	441	0.0001	H-1 → L (77%)
	$S_0 \rightarrow S_2$	3.49	355	0.6662	H → L (87%)
	$S_0 \rightarrow S_3$	4.11	301	0.0006	H → L+1 (93%)

Table 4.2 shows the calculated absorption and emission of SB and complexes in gas phase at wB97X-D/6-311G(d,p). The absorption and emission of SB were showed at 320 and 333 nm with HOMO to LUMO (76%) and HOMO to LUMO (81%), respectively. When SB interacted Ag^+ ion, the absorption and emission were red-shift to 334 and 355 nm. The optical changes when SB interacting to Ag^+ are not obviously observed by naked eyes.

4.1.2 Investigation of 2:1 of SB molecules to metal ion

The orientations of 2 SB molecules and 1 metal ion were designed in 2 orientations as **(1)** and **(2)**. The functional of SB in **(1)** orientation was designed in the similar site of functional group but **(2)** orientation was opposite. Then, each orientation was added the Ag^+ in center of the 2 molecules as presented in before optimization in Figure 4.4 After fully optimization at ground state had performed by B3LYP functional using 6-311G(d,p) and LANL2DZ basis set for organic molecules and Ag^+ in gas phase, respectively, the **(1)** and **(2)** orientation was optimized as shown in after optimization in Figure 4.4. The binding energy was calculated following equation 3.1 as illustrated in Table 4.3. The binding energy indicate that the **(2)** orientation is more stable than **(1)** orientation at the ground state. Furthermore, electrostatic potential surface was determined. Figure 4.5 shows that the center of both orientations is negative moiety which implies to nucleophilic moiety. But (2) orientation can be observed slight more negative charge in the center. According to the negative charge in center of **(2)** orientation, **(2)** orientation is lower BE than **(1)** orientation in Table 4.3.

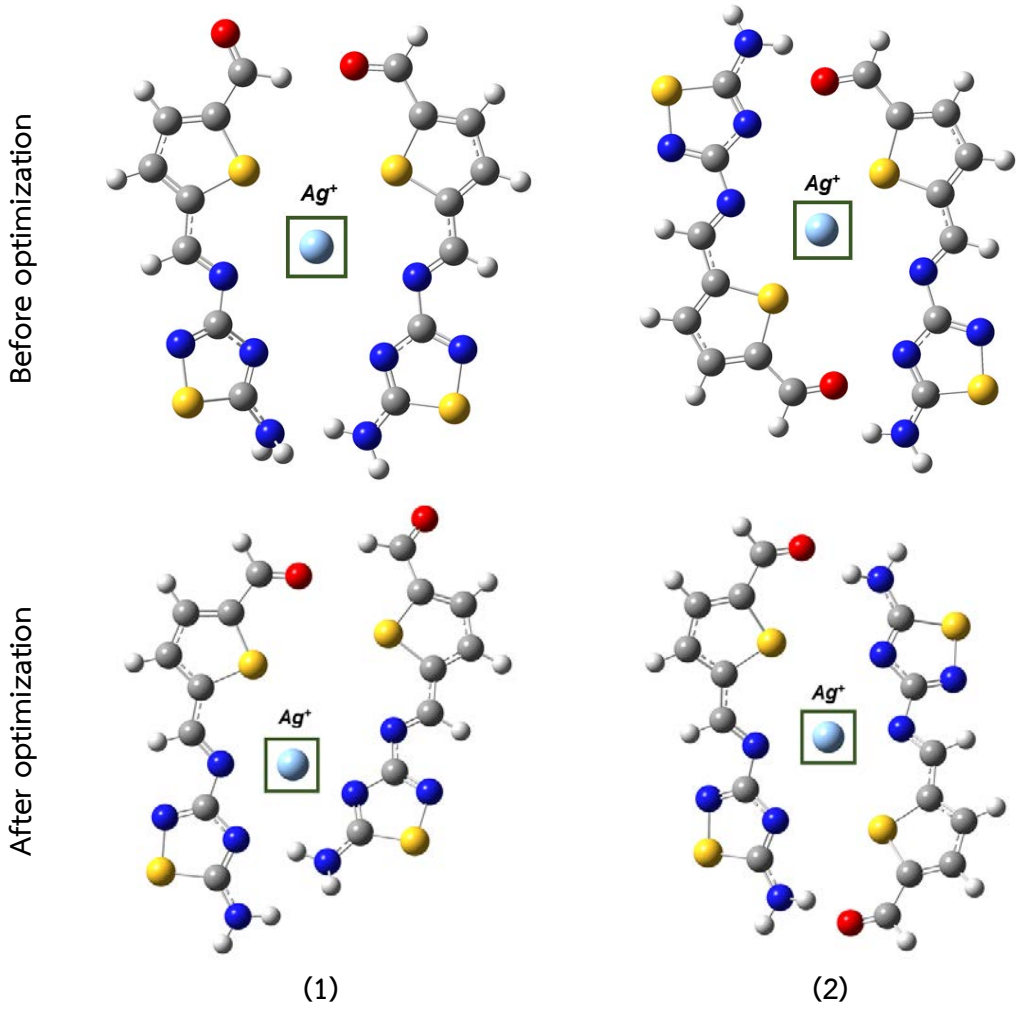

Figure 4.4 The before and after optimization of orientation **(1)** and **(2)** of complexes (2 SB molecules and 1 metal ion)

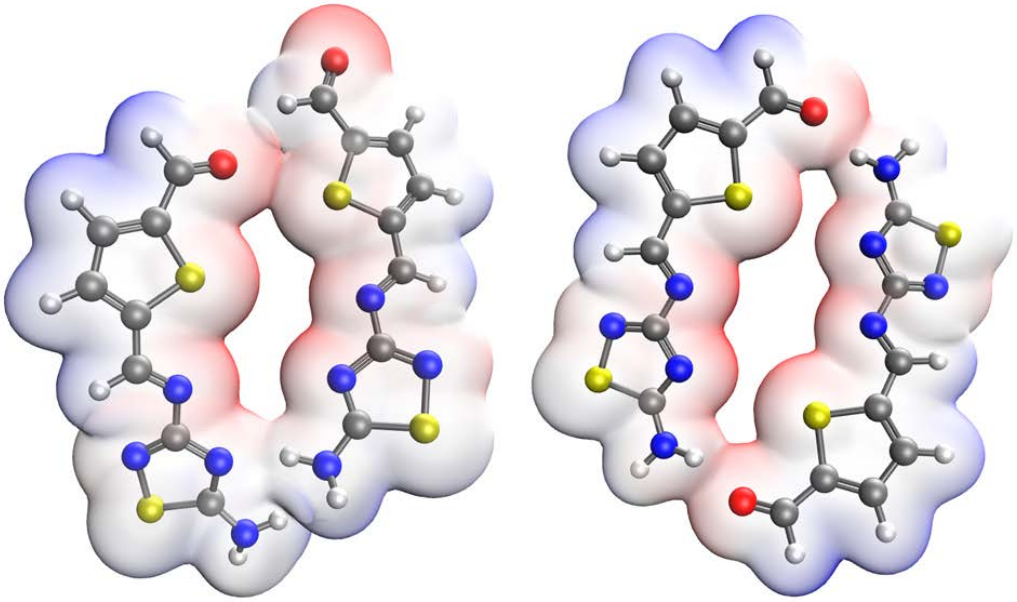

Figure 4.5 The electrostatic potential surfaces (EPS) of **(1)** and **(2)** orientation of 2 SB molecules.

The optical properties, absorbance and emission of complex, were also determined by wB97XD functional using similar basis set as demonstrated in Figure 4.6. However, the fully optimization at the excited state was performed as well. The energy at the excited state of **(1)** and **(2)** orientation are -2943.61 hartree and -2797.89 hartree, respectively. The energy at excited state of **(1)** orientation is less than **(2)** orientation that implied to the **(1)** orientation is more stable than **(2)** orientation at the excited state. Moreover, the **(2)** orientation could be transition state because of large different energy from others. The absorption peaks of **(1)** and **(2)** orientation are 328 nm and 332 nm, respectively. The **(1)** orientation emission peak is red-shift from the absorption peak to 337 nm. The **(2)** orientation emission peak is 500 nm which is less possibility to emit because it is transition state. After that, absorbance and emission of complexes were calculated. The absorption and emission peaks of complexes are red-shift from bare SB. Although the change in optical properties had found in complexes, it was rather difficult to observe by vision. Because the change in absorbance and emission with 20 nm could not be observed by human eyes.

Table 4.3 The binding energy at ground state of **(1)** and **(2)** orientation.

Orientation	Binding Energy (BE) (kcal/mol)
(1)	-95.59
(2)	-98.24

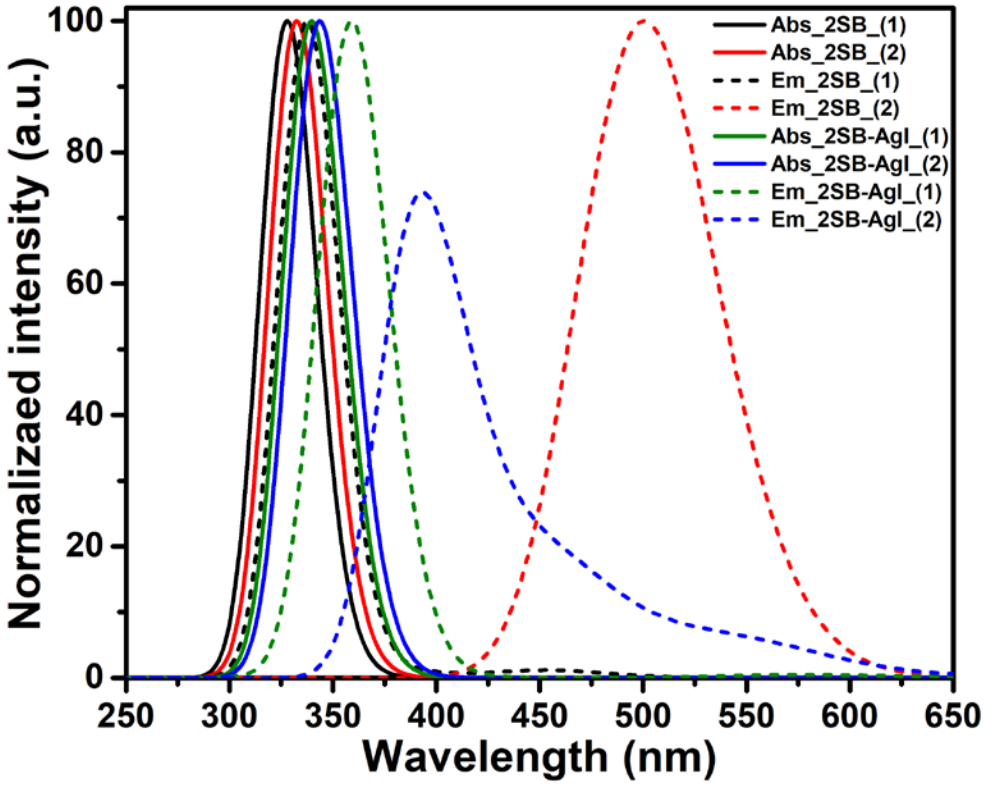

Figure 4.6 The absorbance and emission of 2 SB molecules and complexes

Table 4.4 Calculated absorption and emission wavelength (**λ**), excitation energies (E) and oscillator strengths (f) of the 2 SB and complexes in gas phase at wB97X-D/6-311G(d,p) and TD-DFT.

	Electronic transitions	E (eV)	**λ** (nm)	*f*	Transition state
Abs_2SB_(1)	$S_0 \rightarrow S_1$	3.68	337	0.0001	H-3 → L+1 (64%)
	$S_0 \rightarrow S_2$	3.78	328	0.0270	H-9 → L (34%)
	$S_0 \rightarrow S_3$	3.79	327	0.0349	H-9 → L (31%)
Abs_2SB_(2)	$S_0 \rightarrow S_1$	3.66	338	0.0389	H → L+1 (37%)
	$S_0 \rightarrow S_2$	3.74	331	0.7105	H → L (36%)
	$S_0 \rightarrow S_3$	3.97	312	0.0004	H-11 → L+1 (22%)
Em_2SB_(1)	$S_0 \rightarrow S_1$	3.03	409	0.0001	H-2 → L+1 (58%)
	$S_0 \rightarrow S_2$	3.67	337	0.3847	H → L+1 (82%)
	$S_0 \rightarrow S_3$	3.87	320	0.0016	H-9 → L (61%)
Em_2SB_(2)	$S_0 \rightarrow S_1$	2.46	503	0.0011	H-2 → L (80%)
	$S_0 \rightarrow S_2$	2.62	473	0.0002	H-1 → L (98%)
Abs_2SB-Ag^+_(1)	$S_0 \rightarrow S_1$	3.49	355	0.0001	H-1→L (68%)
	$S_0 \rightarrow S_2$	3.57	347	0.0003	H→L (84%)
	$S_0 \rightarrow S_3$	3.65	339	0.0979	H → L+1 (93%)
Abs_2SB-Ag^+_(2)	$S_0 \rightarrow S_1$	3.57	347	0.0611	H-1 → L (42%)
	$S_0 \rightarrow S_2$	3.62	342	0.6593	H → L (52%)
	$S_0 \rightarrow S_3$	3.80	326	0.0035	H-8 → L (29%)
Em_2SB-Ag^+_(1)	$S_0 \rightarrow S_1$	2.84	436	0.0002	H-5 → L (62%)
	$S_0 \rightarrow S_2$	3.44	360	0.3758	H-3 → L (67%)
	$S_0 \rightarrow S_3$	3.61	343	0.0092	H → L (94%)
Em_2SB-Ag^+_(2)	$S_0 \rightarrow S_1$	2.22	557	0.0017	H-2 → L (82%)
	$S_0 \rightarrow S_2$	2.68	462	0.0052	H-3 → L (83%)

Table 4.4 shows the absorption and emission of 2 SB molecules and complexes. The absorption of 2 SB molecules were absorbed at around 330 nm. Emission of **(1)** and **(2)** orientation emitted at 337 and 503 nm, respectively. Then, Ag+ was added, the absorption and emission were red-shift. However, it cannot be clearly observed by naked eyes.

4.1.3 Investigation of SB-Rho and complexes

The SB-Rho, as shown in Figure 3.1, was designed in 3 orientations (**L1**, **L2**, **L3** and **L4**) and fully optimized at ground state with B3LYP functional using 6-311G(d,p) basis set as illustrated in Figure 4.7. Table 4.5 demonstrates the energy of SB-Rho at all orientations that **L4** are slightly less than others. So, all of orientations are possible to exhibit in each orientation. After that, the TD-DFT was used to determine the absorbance of **L3** with various functional (B3LYP, M06-2x, PBE1PBE, TPSSH, and wB97X-D) to obtain the suitable functional for excited state optimization. Figure 4.8 shows the absorbance of **L3** with various functional. The suitable functionals are M06-2x and wB97X-D because their calculations are close to experimental results. However, wB97X-D was used to optimize and calculate the excited state because it included the non-covalent interactions term in the calculation [37]. The wB97X-D functional was used to determine the absorbance of SB-Rho at all orientations in gas phase. The absorption peak of all orientations is slight shift as shown in Figure 4.9 Then, the Ag^{+} was added to each orientation to determine the binding site of metal ion. The complexes was fully optimized with B3LYP using 6-311G(d,p) and LANL2DZ for organic molecules and Ag^{+}, respectively (Figure 4.7). The binding energy was calculated following the Equation 3.1 as shown in Table 4.6. The **L3-Ag^{+}** complex is the lowest binding energy of -446.75 kcal/mol that could be implied to too strong binding site at ketone in Rhodamine molecule and SB moiety as shown in Figure 4.7. However, the binding energy of all orientations are negative value around -80 kcal/mol which is enough for interacting with SB-Rho. Then, the various heavy metal ions were added to **L3** orientation. The binding energy also was calculated by Equation 3.1 as shown in Table 4.7. The low binding energy can be implied to SB-Rho can interact with metal ions.

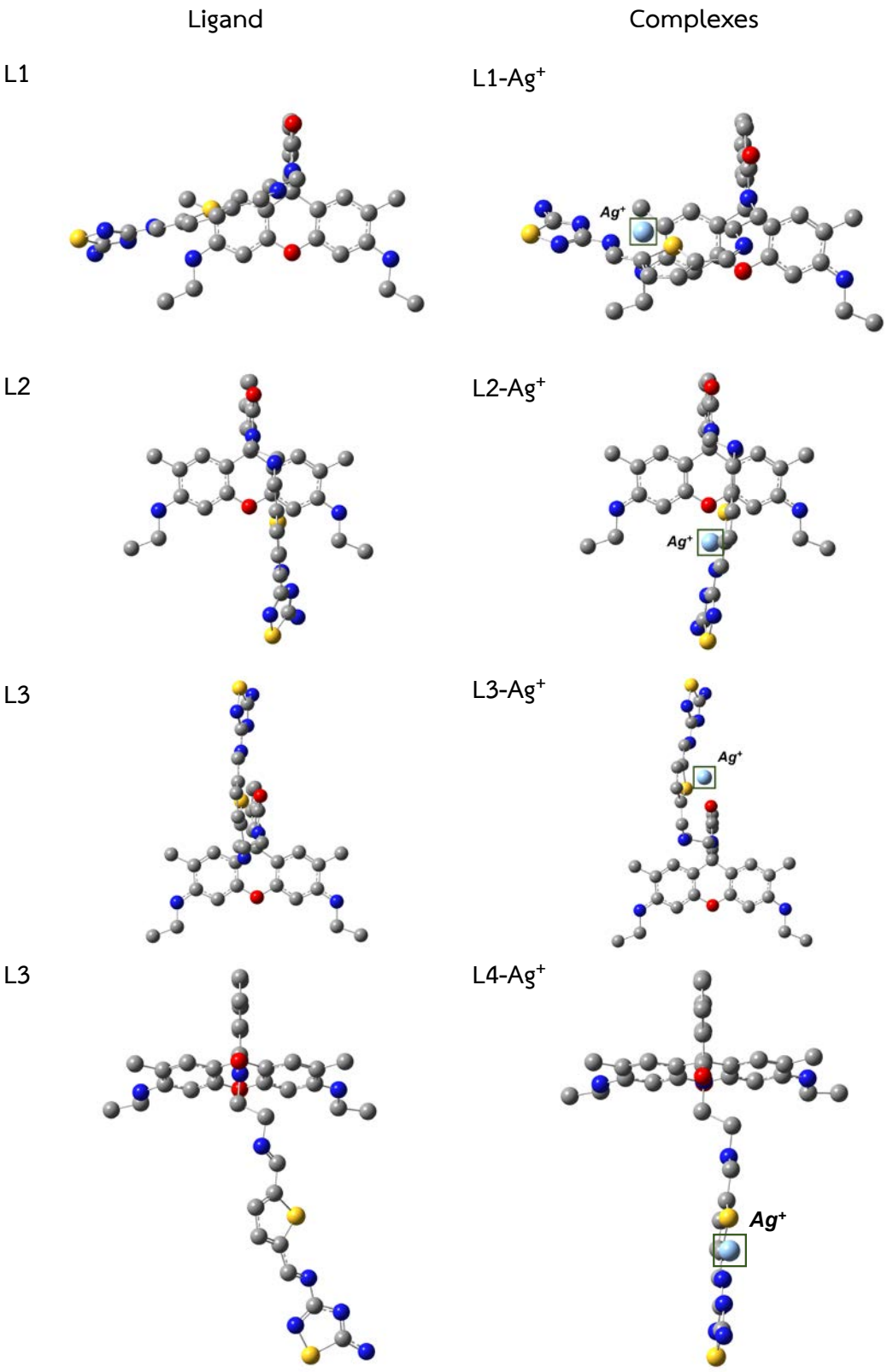

Figure 4.7 The orientation of SB-Rho (**L1**, **L2**, **L3**, and **L4**) and complexes.

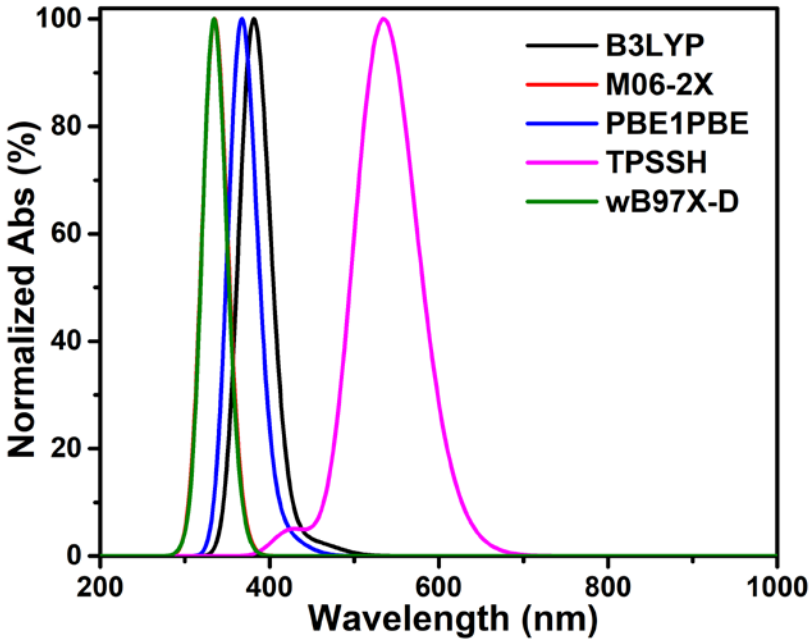

Figure 4.8 The calculated absorbance of **L3** using B3LYP, M06-2x, PBE1PBE, TPSSH, and wB97X-D with 6-311G(d,p) basis set.

Table 4.5 The energy of **L1**, **L2**, **L3** and **L4**.

	Energy (hartree)
L1	-2778.9039
L2	-2778.8962
L3	-2778.3430
L4	-2778.9044

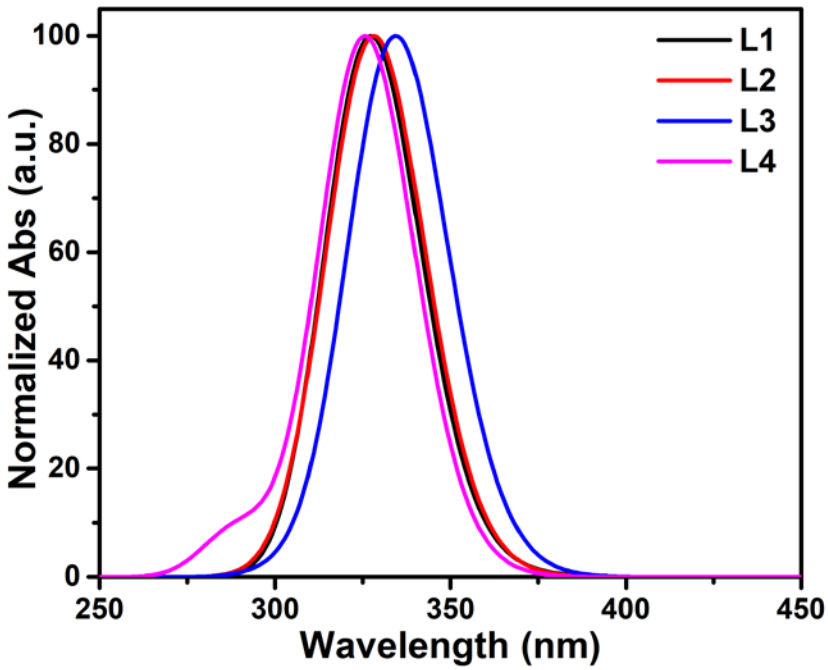

Figure 4.9 Calculated absorbance of **L1**, **L2**, **L3** and **L4** using wB97X-D/6-311g(d,p) in gas phase

Table 4.6 The binding energy of complexes.

	Binding energy (BE) (kcal/mol)
L1-Ag^+	-80.78
L2-Ag^+	-84.48
L3-Ag^+	-446.75
L4-Ag^+	-73.23

Table 4.7 The binding energy of complexes.

Complexes		Binding energy (BE) (kcal/mol)
L3	Ag^+	-446.75
	Cu^{2+}	-761.12
	Hg^{2+}	-632.59
	Mn^{2+}	-647.54
	Ni^{2+}	-720.78
	Pb^{2+}	-587.19
	Zn^{2+}	-671.80

4.2 Experimental study

The SB molecule was synthesized following the previous literature [36]. Then, the SB-Rho was successfully synthesized, after Rhodamine 6G had been functionalized with ethylenediamine as shown in Figure 3.1. The SB-Rho was characterized with ^{1}H NMR, FTIR.

4.2.1 Characterization of SB-Rho

The SB-Rho was successfully synthesized by following the procedure as mentioned above. The molecular structure of SB-Rho was characterized by FTIR and ^{1}H NMR. Figure 4.9 shows the FTIR spectra that confirm characteristic peaks of Rhodamine 6G which are stretching vibration of C-O at 1715 cm^{-1}, stretching peaks of C-H (CH_2) at 2976 and 2876 cm^{-1}, bending vibration of CH_2 in aromatic at 1643, 1440 and 1360 cm^{-1}, and stretching vibration of C-H (CH_3) at 3631 cm^{-1} [38-40]. The FTIR

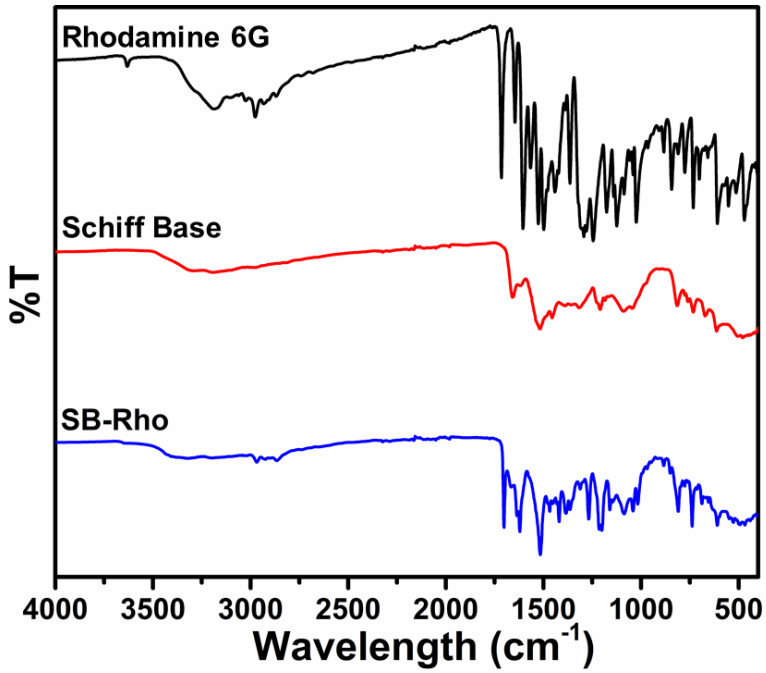

Figure 4.10 The FTIR spectra of Rhodamine 6G, Schiff base, and Schiff base-Rhodamine 6G (SB-Rho)

spectra of SB appear the characteristic peaks at 1656, 1617, 1390, and 1317 cm^{-1} which relate to stretching vibration of imine (C=N), bending vibration of NH_2, bending vibration of C-H in aldehyde group, and stretching vibration of aromatic amine (C-N), respectively [41]. Next, FTIR spectra of SB-Rho shows characteristic peaks both of Rhodamine 6G

and SB. Thus, FTIR spectra confirmed that SB-Rho was successfully synthesized. Another characterization of SB-Rho is ^{1}H NMR (Figure 4.10 and 4.11). The ^{1}H NMR provide peak that confirm rhodamine 6G functionalized with ethylene diamine at δ; 1.22 (-CH_3), 1.87 (-CH_3), 2.16 (-CH_2-), 2.94 (-CH_2-), 3.13 (-NH_2), 6.09 (-NH-). Then the structure of SB-Rho was also confirmed by ^{1}H NMR as illustrated in Figure 4.11. The characteristic peak of ^{1}H NMR of SB-Rho appears at δ; 1.22 (-CH_3), 1.83 (-CH_3), 3.19 (-CH_3), 3.80 (-CH_2), 3.92 (-CH_2), 5.06 (-NH_2), 9.85 (-CH=N), 10.02 (-CH=N).

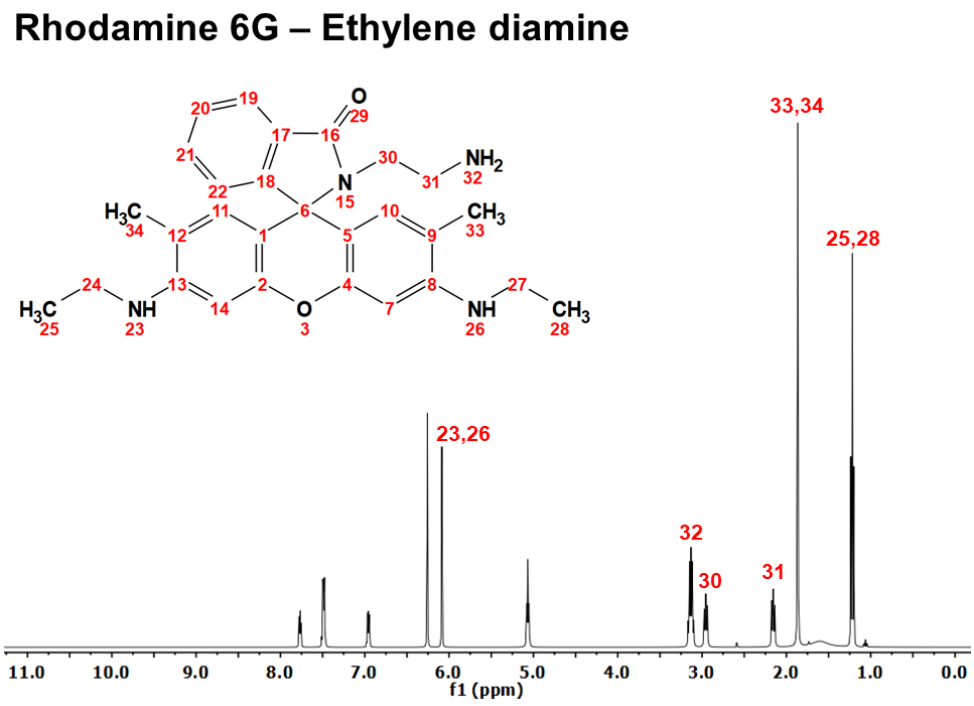

Figure 4.11 ^{1}H NMR spectra of Rhodamine 6G functionalized with ethylene diamine

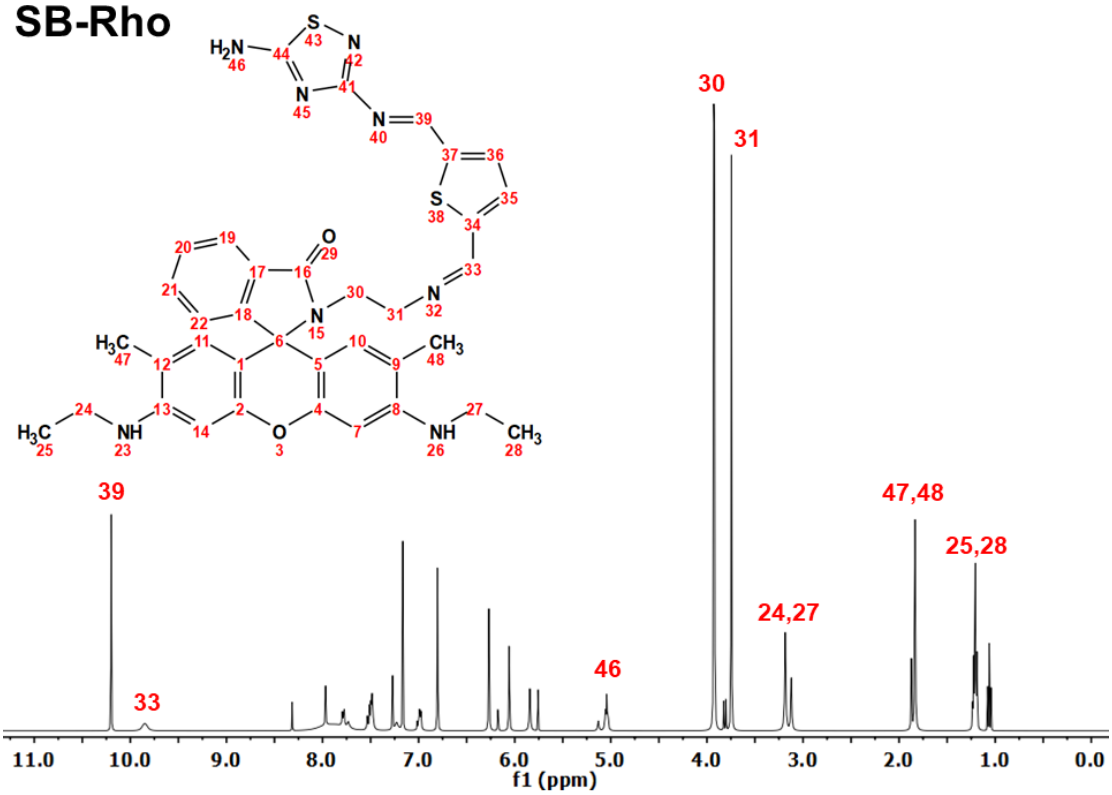

Figure 4.12 ^{1}H NMR spectra of SB-Rho

4.2.2 Heavy metal detection

Firstly, the solvent effect was performed by using various solvent (acetone, acetonitrile, dimethyl sulfoxide (DMSO), ethanol, ethyl acetate, methanol, and mixed solvent of 1:1 or 1:1:1 ratio). However, the SB-Rho can be completely dissolved in only DMSO and mixed solvent of methanol: deionized water (DI): Ethyl acetate. All of

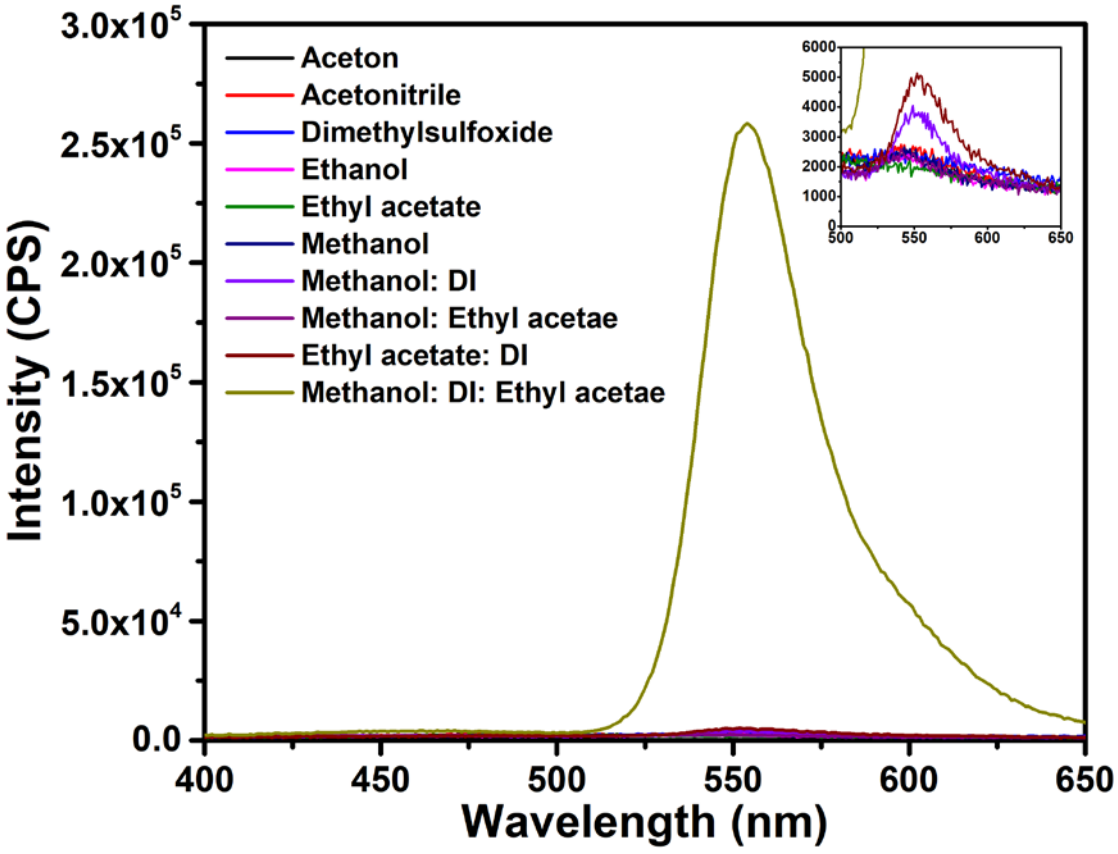

Figure 4.13 Emission spectra with various solvents

solvents have emission around at 550 nm, but mixed solvent of methanol: DI: ethyl acetate obviously provides the highest fluorescent intensity as illustrated in Figure 4.12. So, mixed solvent of methanol: DI: ethyl acetate will be used in this study due to completely dissolve. Because isolated molecule which happened when completely dissolve can represent the calculated SB-Rho calculation with 1 molecule in gas phase. Next, the anion effect was carried out by using various anion (Cl^-, $COOH^-$, NO_3^-, SO_4^{2-}). Absorbance and fluorescence were measured as shown in Figure 4.13 and 4.14. Both of optical properties are not change in energy and slightly change in intensity which doesn't affect to heavy metal ion detection.

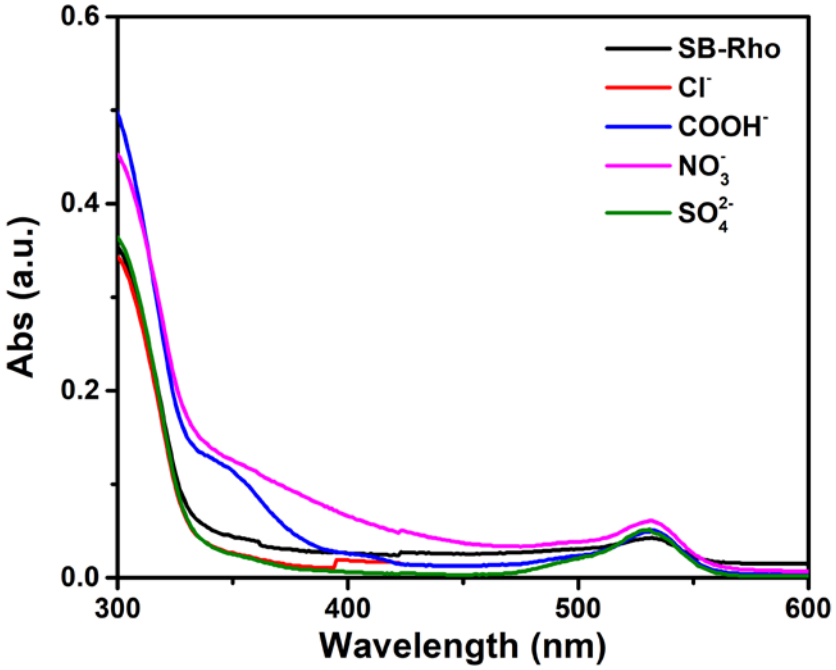

Figure 4.14 Absorbance of SB-Rho in various anion (Cl^-, $COOH^-$, NO_3^-, SO_4^{2-}).

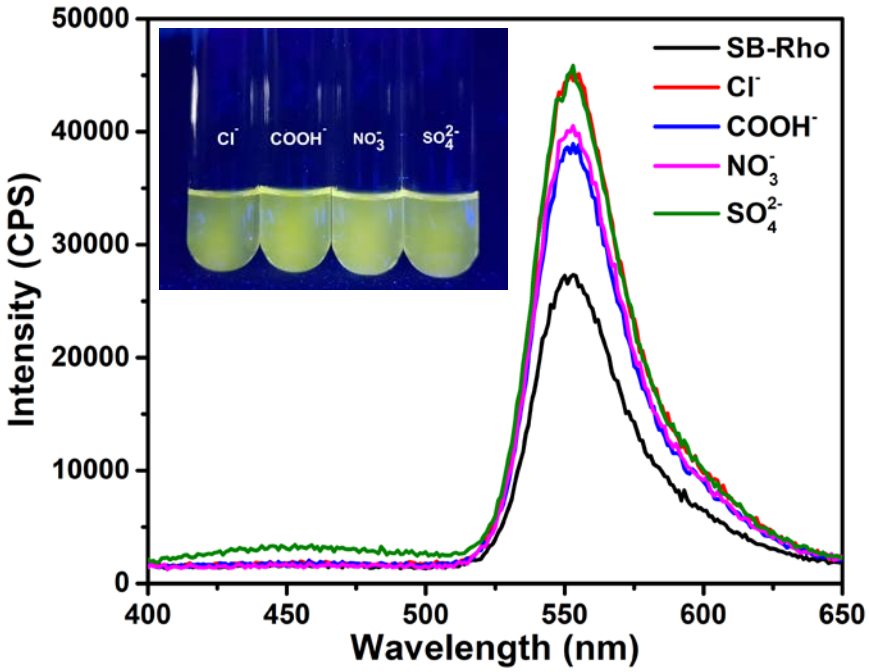

Figure 4.15 Fluorescence of SB-Rho in various anion (Cl^-, $COOH^-$, NO_3^-, SO_4^{2-}).

Figure 4.15 shows the fluorescence of SB-Rho, solvent and complex. The various heavy metal ions were prepared in stock solution at 1 mM in mixed solution. Fluorescence was measured at 400 μM of heavy metal ion and 8 μM SB-Rho with excitation 350 nm and slit width of 1 nm at room temperature. The fluorescent peak

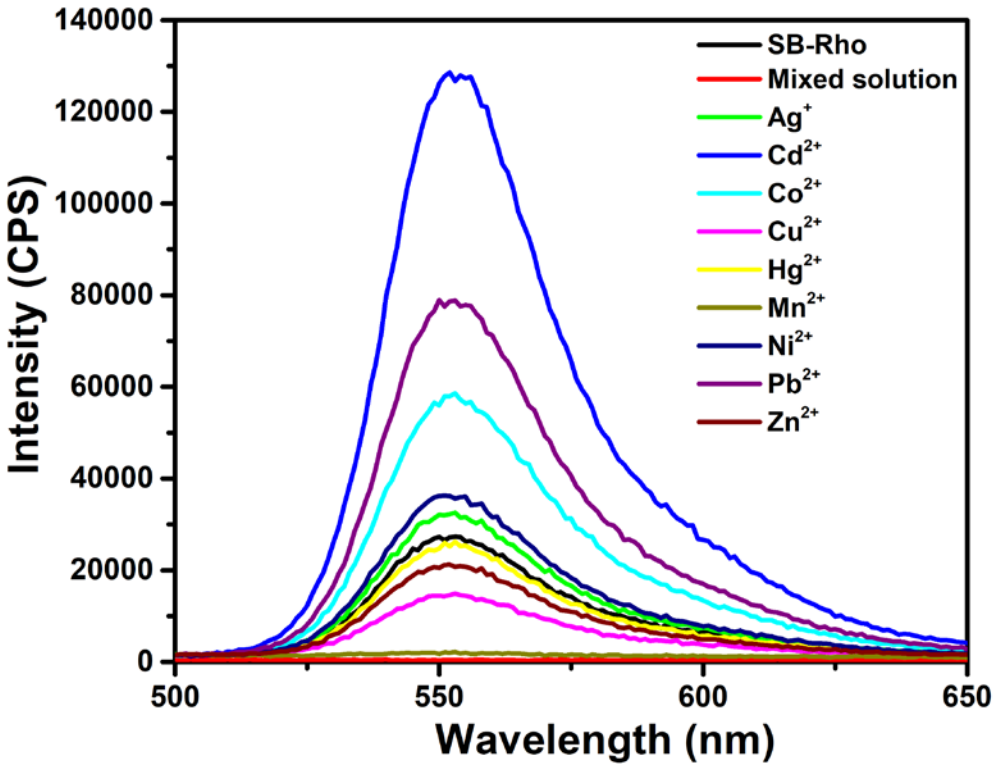

Figure 4.16 Fluorescent spectra of SB-Rho (8 μM) with Mn^{2+} and various cations in mixed solution.

of SB-Rho appears at 550 nm. When various heavy metal ions were added in the solution, the peak at 550 nm changed in intensity. All of complexes are change in intensity which the Cd^{2+} complex provides the highest intensity. Owing to change in fluorescent intensity in all complexes, the heavy metal ion detection could not be completely distinguished. However, the only one which quenches the fluorescent intensity is Mn^{2+}. The imine groups can improve the binding of meta ions Mn^{2+}, classified as “hard” metal [42]. Furthermore, Figure 4.17 illustrates photograph of SB-Rho and complexes which clearly observed change in color of solution in room light and under UV light. Cd^{2+}, Co^{2+} and Pb^{2+} are change the color solution from colorless

to pink. As illustrated in Figure 4.17(b), only Mn^{2+} solution found quenching fluorescence. Thus, the SB-Rho could be sensitive with Mn^{2+}.

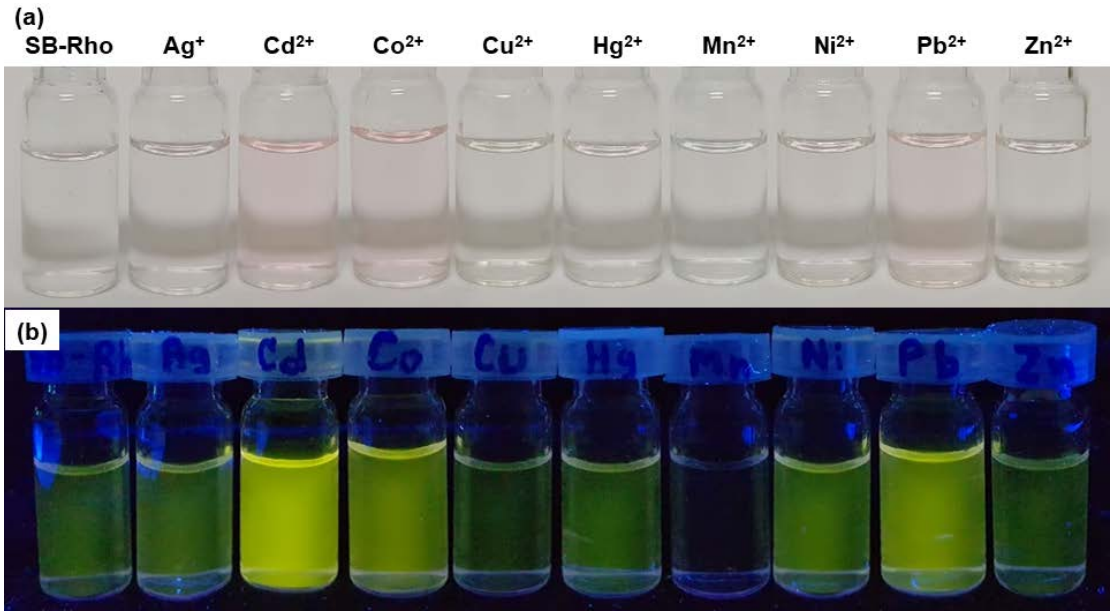

Figure 4.17 Photographs of SB-Rho (8 μM) upon addition of 400 μM of various metal ions in mixed solvent (methanol: DI: ethyl acetate) taken under (a) room light, (b) UV light.

Figure 4.18 demonstrate the fluorescence "Turn-Off" mechanism for Mn^{2+} detection by SB-Rho. The electron distribution was calculated at HOMO and LUMO of SB-Rho and SB-Rho-Mn^{2+}. The fluorescence at 550 nm of SB-Rho is the photoinduced electron transfer (PET) which electron distribution from rhodamine 6G moiety transfer to Schiff base moiety. Because of the interaction of Mn^{2+} to the SB-Rho at oxygen donor and imine groups, the electron transfer between rhodamine 6G and Schiff base was disrupted due to blocking the PET mechanism, leading to a significantly quenching fluorescence emission.

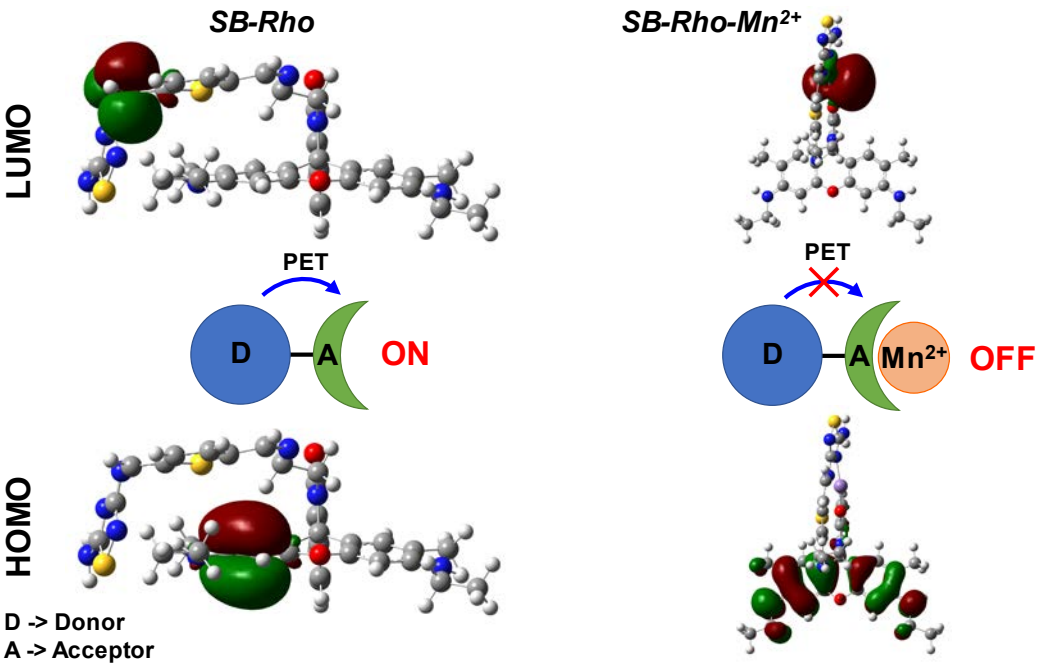

Figure 4.18 The schematic demonstration of Fluorescence "Turn-Off" mechanism for Mn2+ Detection by SB-Rho.

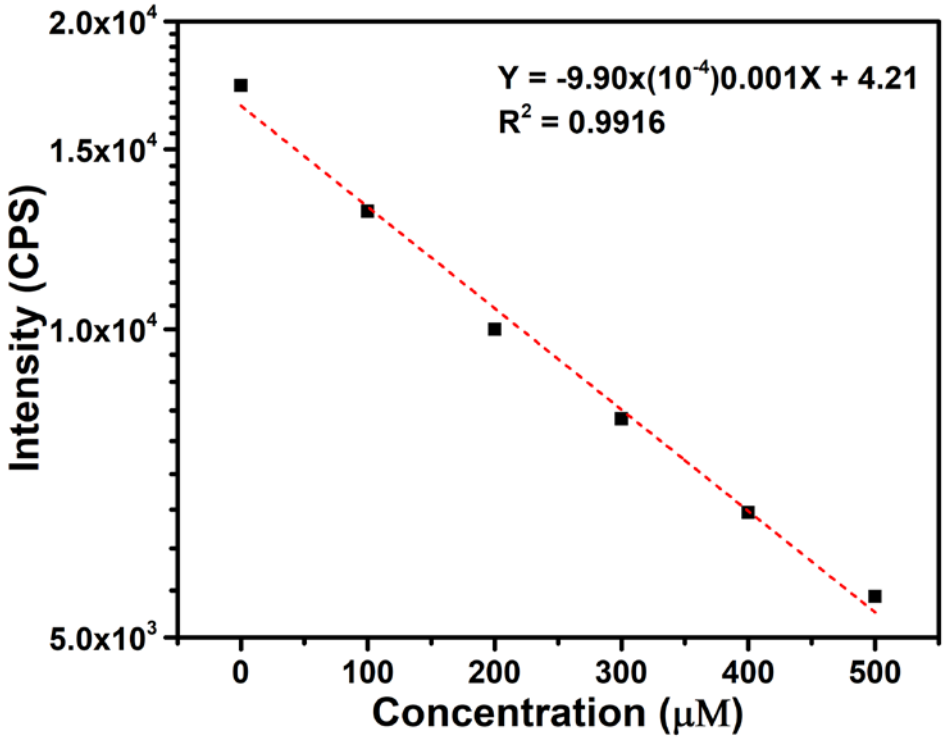

Figure 4.19 Fluorescent intensity at 550 nm for SB-Rho as a function of the concentration of Mn^{2+} ion. The concentration of Mn^{2+} are 100, 200, 300, 400, and 500 μM

Then, the linear fluorescence quenching of SB-Rho (8 μM) toward amounts of Mn^{2+} added was obtained over the range of 0-500 μM (R^2 = 0.99) as shown in Figure 4.19. The limit of detection (LOD) was calculated following the equation

$$LOD = \frac{3.3 \times \sigma}{S}. \quad (4.1)$$

Where σ represents standard derivative of response and S is slope of calibration curve [43]. LOD of SB-Rho to Mn^{2+} is 7 μM.

After that, the kinetic characteristic of the detected system was investigated (Figure 4.20). No obvious fluorescence variation of SB-Rho (8 μM) at 550 nm were observed even over a period of 10 min. The real-time determination is necessary in sensor. In this study, time evolution was investigated with responses of SB-Rho (8 μM) in the presence of 400 μM of Mn^{2+} in mixed solution. The results illustrated that fluorescence of SB-Rho remarkably decreased to 10 percent of initial fluorescence intensity within the first 40 sec. That can be implied the response time of SB-Rho to

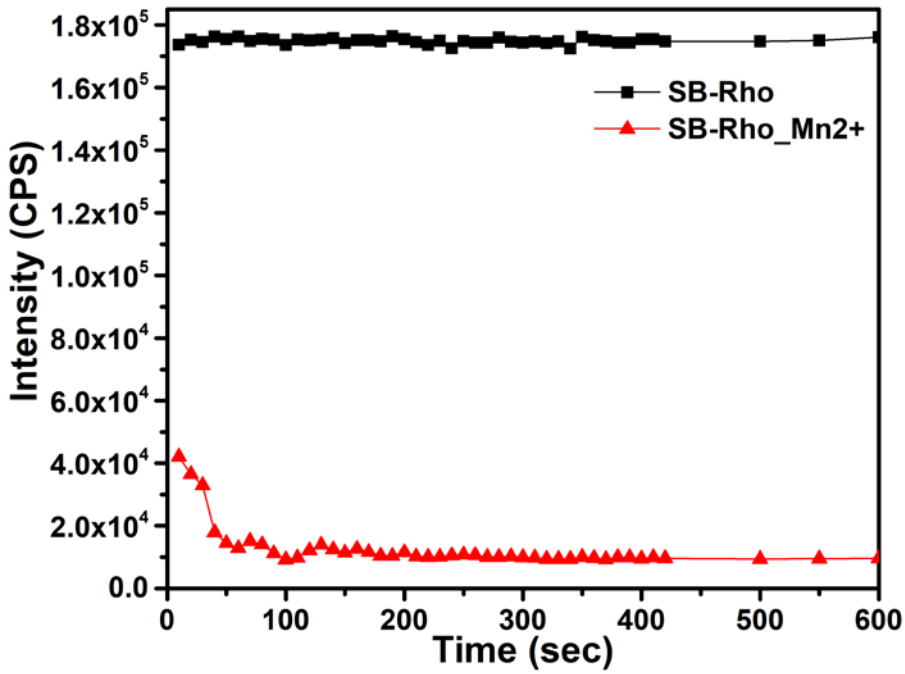

Figure 4.20 Fluorescent intensity (550 nm) of SB-Rho (8 μM) in mixed solution of different time in the absence and presence of Mn^{2+} (400 μM)

Mn^{2+} is 40 sec and saturation at 50 sec. Therefore, SB-Rho could be used in real-time determination of Mn^{2+} in the environmental analysis. A much decrease up to 17.5-fold

of complex from bare SB-Rho can be distinguishably obovered. Furthermore, the binding stoichiometry of SB-Rho with Mn^{2+} was performed by a Job's plot. Keeping the concentration of SB-Rho and Mn^{2+} at 0.2 mM (Figure 4.21), the volume ratio of Mn^{2+} was varied from 0 to 1. The fluorescence intensity of SB-Rho provided maximum when the volume ratio of SB-Rho was 0.7. Which could be implied to 2:1 stoichiometry for the SB-Rho-Mn^{2+} complex.

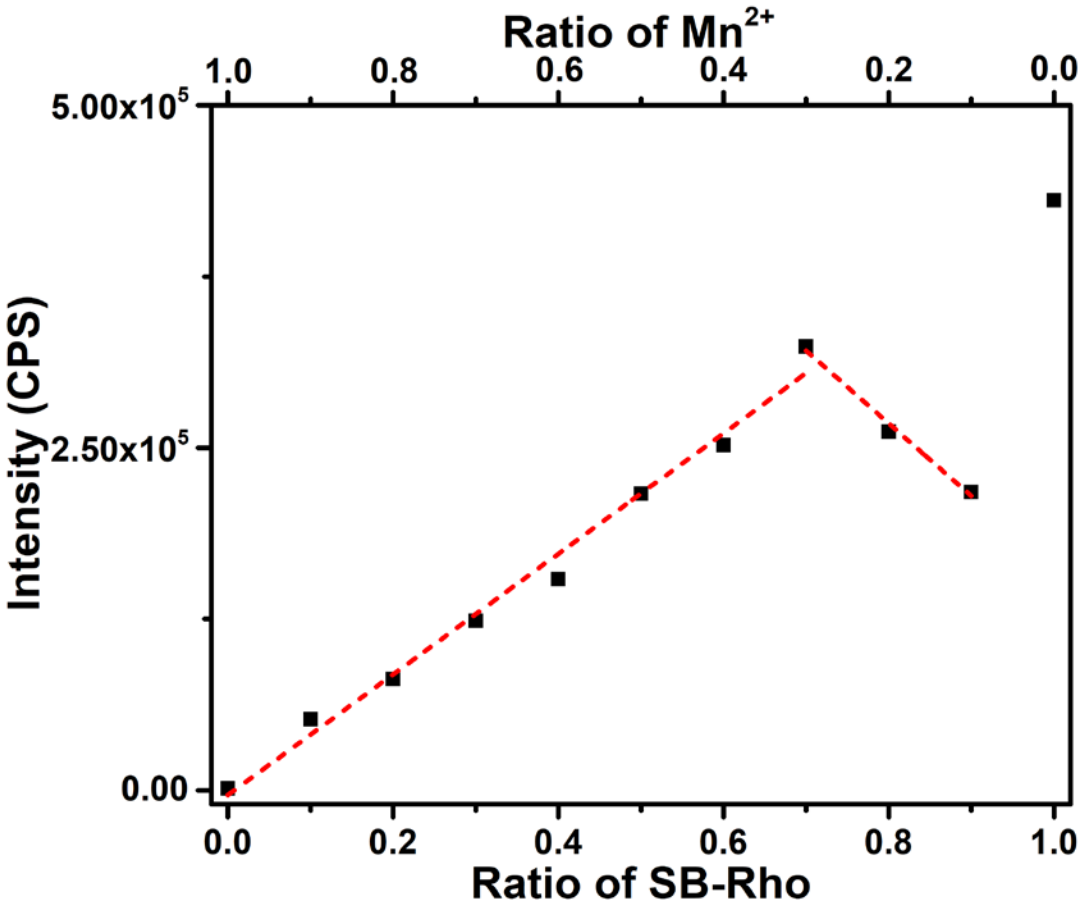

Figure 4.21 Job's plot of SB-Rho and Mn^{2+} by keeping concentration of 0.2 mM.

CHAPTER 5

CONCLUSION

The theoretical calculation and experimental study was investigated in this work. First, the theoretical study was calculated the interaction between SB and Ag^+ in ratio of 1:1 and 2:1 of SB molecule to metal ion. The fully optimization were carried out by B3LYP using 6-311G(d,p) and LANL2DZ for organic molecule and metal ion, respectively. As the ratio of 1:1, the binding energy indicated that the binding site of metal ion was position 3 with -63.78 kcal/mol. Then, the absorbance and emission of SB and complexes were determined by TD-DFT with wB97X-D functional using similar basis set. The absorption peak of SB was 320 nm. When it interacted with Ag^+, the absorbance and emission were red-shift. Next, the ratio of 2:1 was investigated by fully optimization at ground state with B3LYP functional and same basis set. The orientations were divided into 2 orientations (**(1)** and **(2)**). At ground state, when SB interacted to metal ion, **(2)** orientation had lower binding energy. However, at excited state, **(1)** orientation has lower energy than **(2)** orientation. The absorbance and emission peak of **(1)** and **(2)** were also red-shift, when interacted with metal ion. Finally, in theoretical study, the SB-Rho and complexes were studied. The 3 orientations were obtained from SB-Rho (**L1**, **L2** and **L3**). The fully optimization at ground state were carried out by B3LYP functional using same basis set. All of orientations were not remarkably different. But **L3-Ag^+** was the lowest binding energy.

The experimental study was performed by successfully synthesizing the SB functionalized with Rhodamine 6G. The FTIR confirmed the SB-Rho molecular structure by stretching vibration of imine group (C=N). Additionally, ^{1}H NMR also confirmed the molecular structure of SB-Rho by characteristic peaks. Then, the heavy metal detection was investigated. Firstly, solvent effect was performed by using various solvents. The methanol: DI: ethylacetate provided the highest fluorescence. Next, anion effect was carried out. The results show that the anion was not affect to fluorescence. Finally,

various heavy metal ions were studied. The results demonstrated that only Mn^{2+} found quenching fluorescence. Then, the linear fluorescence quenching of SB-Rho toward amounts of Mn^{2+} added was obtained over the range of 0-500 μM. LOD of SB-Rho to Mn^{2+} is 7 μM. The response time is only 40 sec. The binding stoichiometry of SB-Rho with Mn^{2+} was 2:1 stoichiometry. Thus, the SB-Rho could be sensitive with Mn^{2+}.

REFERENCES

1. Turdean, G.L., *Design and Development of Biosensors for the Detection of Heavy Metal Toxicity.* International Journal of Electrochemistry, 2011. **2011**: p. 1-15.
2. Gumpu, M.B., et al., *A review on detection of heavy metal ions in water – An electrochemical approach.* Sensors and Actuators B: Chemical, 2015. **213**: p. 515-533.
3. Singh, A., et al., *Health risk assessment of heavy metals via dietary intake of foodstuffs from the wastewater irrigated site of a dry tropical area of India.* Food Chem Toxicol, 2010. **48**(2): p. 611-9.
4. Duruibe, J., O. M. O. C, and J. Egwurugwu, *Heavy Metal Pollution and Human Biotoxic Effects*. Vol. 2. 2007. 112-118.
5. Jin, S., et al., *Effect of the magnetic core size of amino-functionalized Fe 3 O 4 -mesoporous SiO 2 core-shell nanoparticles on the removal of heavy metal ions.* Colloids and Surfaces A: Physicochemical and Engineering Aspects, 2017. **531**: p. 133-140.
6. Squadrone, S., et al., *Mercury and selenium in European catfish (Silurus glanis) from Northern Italian Rivers: can molar ratio be a predictive factor for mercury toxicity in a top predator?* Chemosphere, 2015. **119**: p. 24-30.
7. Marambio-Jones, C. and E.M.V. Hoek, *A review of the antibacterial effects of silver nanomaterials and potential implications for human health and the environment.* Journal of Nanoparticle Research, 2010. **12**(5): p. 1531-1551.
8. Mason, L.H., J.P. Harp, and D.Y. Han, *Pb neurotoxicity: neuropsychological effects of lead toxicity.* Biomed Res Int, 2014. **2014**: p. 840547.
9. Walter, E., et al., *Manganese toxicity in critical care: Case report, literature review and recommendations for practice.* J Intensive Care Soc, 2016. **17**(3): p. 252-257.
10. Stuntz, E., et al., *Endogenous Two-Photon Excited Fluorescence Imaging Characterizes Neuron and Astrocyte Metabolic Responses to Manganese Toxicity.* Sci Rep, 2017. **7**(1): p. 1041.

11. Baker, M.G., et al., *Neurological outcomes associated with low-level manganese exposure in an inception cohort of asymptomatic welding trainees.* Scand J Work Environ Health, 2015. **41**(1): p. 94-101.
12. Berg, K.E., et al., *Manganese Detection Using Stencil-printed Carbon Ink Electrodes on Transparency Film.* Electroanalysis, 2016. **28**(4): p. 679-684.
13. Hojabri, H., et al., *Determination of metal ions using ion chromatography and indirect amperometric detection.* Analytical Chemistry, 1987. **59**(1): p. 54-57.
14. Rai, A., et al., *Rhodamine hydrazone as OFF–ON–OFF type selective sequential sensor of Al3+ and N3− ions.* Journal of Photochemistry and Photobiology A: Chemistry, 2016. **319-320**: p. 78-86.
15. Ghosh, P., et al., *Colorimetric and fluorimetric response of Schiff base molecules towards fluoride anion, solution test kit fabrication, logical interpretations and DFT-D3 study.* Phys Chem Chem Phys, 2015. **17**(31): p. 20288-95.
16. Benabid, S., et al., *Electrochemical and DFT studies of a new synthesized Schiff base as corrosion inhibitor in 1MHCl.* Measurement, 2017. **99**: p. 53-63.
17. Liu, Y., et al., *Cd2+-triggered amide tautomerization produces a highly Cd2+-selective fluorescent sensor across a wide pH range.* Dyes and Pigments, 2016. **133**: p. 339-344.
18. Pogány, L., et al., *Four cobalt(III) Schiff base complexes – Structural, spectroscopic and electrochemical studies.* Inorganica Chimica Acta, 2017. **462**: p. 23-29.
19. Hossain, S., C.M. Zakaria, and E.Z. Kudrat, *Structural and biological activity studies on metal complexes containing thiosemicarbzone and isatin based schiff base: A review.* Asian Journal of Research in Chemistry, 2017. **10**(1): p. 6.
20. Abu-Dief, A.M. and I.M.A. Mohamed, *A review on versatile applications of transition metal complexes incorporating Schiff bases.* Beni-Suef University Journal of Basic and Applied Sciences, 2015. **4**(2): p. 119-133.
21. Kumar, G., et al., *Synthesis, spectral characterization and antimicrobial evaluation of Schiff base Cu (II), Ni (II) and Co (II) complexes.* Eur J Med Chem, 2010. **45**(7): p. 3056-62.

22. Kumari, S. and G.S. Chauhan, *New cellulose-lysine Schiff-base-based sensor-adsorbent for mercury ions.* ACS Appl Mater Interfaces, 2014. **6**(8): p. 5908-17.
23. Shoora, S.K., A.K. Jain, and V.K. Gupta, *A simple Schiff base based novel optical probe for aluminium (III) ions.* Sensors and Actuators B: Chemical, 2015. **216**: p. 86-104.
24. Tyagi, P., et al., *Design, spectral characterization, DFT and biological studies of transition metal complexes of Schiff base derived from 2-aminobenzamide, pyrrole and furan aldehyde.* Spectrochim Acta A Mol Biomol Spectrosc, 2015. **143**: p. 1-11.
25. Beija, M., C.A. Afonso, and J.M. Martinho, *Synthesis and applications of Rhodamine derivatives as fluorescent probes.* Chem Soc Rev, 2009. **38**(8): p. 2410-33.
26. Li, H., et al., *An acid catalyzed reversible ring-opening/ring-closure reaction involving a cyano-rhodamine spirolactam.* Org Biomol Chem, 2013. **11**(11): p. 1805-9.
27. Kim, H.N., et al., *A new trend in rhodamine-based chemosensors: application of spirolactam ring-opening to sensing ions.* Chem Soc Rev, 2008. **37**(8): p. 1465-72.
28. Sun, S., et al., *Naphthylamine-rhodamine-based ratiometric fluorescent probe for the determination of Pd2+ ions.* Org Lett, 2014. **16**(4): p. 1132-5.
29. Liu, Z., W. He, and Z. Guo, *Metal coordination in photoluminescent sensing.* Chem Soc Rev, 2013. **42**(4): p. 1568-600.
30. Neupane, L.N., et al., *Selective and Sensitive Detection of Heavy Metal Ions in 100% Aqueous Solution and Cells with a Fluorescence Chemosensor Based on Peptide Using Aggregation-Induced Emission.* Anal Chem, 2016. **88**(6): p. 3333-40.
31. Nhan, D.T., et al., *A Benzothiazolium-derived Colorimetric and Fluorescent Chemosensor for Detection of Hg2+ Ions.* Chemistry Letters, 2017. **46**(1): p. 135-138.
32. Capelle, K., *A bird's-eye view of density-functional theory*. Vol. 36. 2006.

33. Amat, A., et al., *DFT/TDDFT investigation on the UV-vis absorption and fluorescence properties of alizarin dye.* Phys Chem Chem Phys, 2015. **17**(9): p. 6374-82.
34. Frisch, M.J., et al., *Gaussian 09*. 2009, Gaussian, Inc.: Wallingford, CT, USA.
35. Piyawan, L., S. Songwut, and P. Darinee, *Schiff Base modified on CPE electrode and PCB gold electrode for selective determination of silver ion.* Journal of Physics: Conference Series, 2017. **901**(1): p. 012080.
36. Leepheng, P., S. Suramitr, and D. Phromyothin, *Schiff Base modified on CPE electrode and PCB gold electrode for selective determination of silver ion.* Journal of Physics: Conference Series, 2017. **901**: p. 012080.
37. Chai, J.-D. and M. Head-Gordon, *Long-range corrected hybrid density functionals with damped atom-atom dispersion corrections.* Physical Chemistry Chemical Physics, 2008. **10**(44): p. 6615-6620.
38. Cao, J., et al., *Luminescent Rhodamine 6G/silica hybrid nanofibers with potential temperature sensing ability.* Journal of Non-Crystalline Solids, 2018. **482**: p. 40-45.
39. Li, Z., et al., *Removal of rhodamine 6G with different types of clay minerals.* Chemosphere, 2018. **202**: p. 127-135.
40. Al Dwayyan, A.S., et al., *Structural and spectral investigations of Rhodamine (Rh6G) dye-silica core–shell nanoparticles.* Optical Materials, 2012. **34**(5): p. 761-768.
41. Vardhan, H., et al., *Dynamic imine chemistry in metal–organic polyhedra.* RSC Advances, 2015. **5**(82): p. 67011-67030.
42. Mao, X., et al., *Bipyrene-functionalized graphene as a "turn-on" fluorescence sensor for manganese(II) ions in living cells.* ACS Appl Mater Interfaces, 2013. **5**(3): p. 592-7.
43. Shrivastava, A. and V. Gupta, *Methods for the determination of limit of detection and limit of quantitation of the analytical methods.* Chronicles of Young Scientists, 2011. **2**(1): p. 21.

CURRICULUM VITAE

Name-Surname	:	Kunanon Chattrairat
Date of birth	:	17 March 1995
Province	:	Phetchaburi
Education	:	High school, Prommanusorn Phetchaburi
	:	B.En. (Nanomaterial Engineering), college of nanotechnology, King Mongkut's Institute of Technology Ladkrabang, Bangkok (2013)
	:	M.Sc. (Nanoscience and nanotechnology), college of nanotechnology, King Mongkut's Institute of Technology Ladkrabang, Bangkok (2017)
Experience	:	Exchange student summer training, Kurume KOSEN, Japan (2016)
	:	Participant of 5th ASEAN Synchrotron science camp (2016)
	:	Exchange student, IMS, Japan (2018)
	:	Polymeric selective membranes for non-enzymatic detection of urea and organic compounds, patent No. 1501000653 (2015)
Presentation	:	Quantum chemical study of Thiadiazole molecular sensors for detection of heavy metal, A calculation, International Conference on Science Technology of Emerging Materials (STEMa2016)

: Investigation of functional graphene/cypermethrin pesticide molecules by using DFT calculation (NanoKorea2017)

: A theoretical study of small schiff base complexes with heavy metal (ANSCSE21, 2017)

Publication : Investigation of functional graphene/cypermethrin pesticide molecules by using density functional theory calculation (Journal of nanoscience and nanotechnology, Vol. 18, 6786-6790, 2018)